이학박사학위논문

# Effect of Electric Field on Condensed-Phase Molecular Systems

# 응집계 분자 환경에서 전기장 효과 연구

2017년 8월

서울대학교 대학원

화학부 물리화학전공

신성환

Ph. D Dissertation

# Effect of Electric Field on Condensed-Phase Molecular Systems

Supervisor: Prof. Heon Kang

Major: Physical Chemistry

August 2017

By Sunghwan Shin

School of Chemistry

College of Natural Science

Seoul National University

# Abstract

# Effect of Electric Field on Condensed-Phase Molecular Systems

Sunghwan Shin
School of Chemistry, Physical Chemistry
College of Natural Science
Seoul National University

In this dissertation, I studied the effect of electric field on a condensed-phase molecular system. Many experiments have been performed for the investigation of field-induced phenomena, but only a few experiments are available for well-defined experimental conditions with strong electric field. We invented the “ice film capacitor method,” which can apply strong electric field across a frozen molecular film. The effect of the electric field was examined using this method.

Chapter I introduces various experimental methods that are currently used to study field-induced phenomena. The advantages of the ice film capacitor method over other existing technique are briefly mentioned.

In chapter II, the experimental methods used for the study in this

thesis are explained. The detailed procedure of the ice film capacitor method and the basic principle of reflection absorption IR spectroscopy are introduced. Instrumentation of the methods is also described.

In chapter III, the conformational change of 1, 2-dichloroethane (DCE) is investigated under the external electric field. Reflection absorption infrared spectroscopy was used for monitoring the molecular changes such as gauche/trans conversion and the reorientation of gauche-DCE. Trans-DCE molecules converted to gauche-DCE under an external electric field, and this conversion led to the reorientation of gauche-DCE along the electric field. The field-induced changes were occurred at 50 - 90 K, but not at 8 K, indicating that both thermal and electrostatic energies are needed to induce the conformational changes in a frozen molecular film.

In chapter IV, the field-induced dissociation of acetic acid (AA) is studied using the ice film capacitor method. The dissociation of acid was monitored by using infrared spectroscopy and the mechanism of field-induced acid dissociation was discussed. AA molecules were dissociated into acetate ions by the external electric field at an acid-base interface. The amount of field-induced dissociation depended on the direction of the applied electric field, which suggests that the reaction was aided by the reorientation of reagent molecules. The effect of molecular size was studied by comparing the results of formic acid and propionic acid with those obtained for AA. The dissociation of smaller acids was more enhanced, supporting our interpretation that field-induced dissociation occurred via molecular reorientation.

Keywords : electric field, ice film capacitor, surface charging, moleculear conformational change, acid base chemistry, molecular reorientation, RAIRS.

*Student number* : 2011-23226

# Contents

**Chapter IV. Field-Induced Acid Dissociation at the Acid-Base Interface**

# List of Figures

expressed by black, red, and blue lines, respectively. The green line indicates the field strength expected from the plate capacitor model.

**Figure 2-6.** Schematic representation of the reflection and transmission at the interface between phases 1 and 2. **F** and **B** indicate the electric and magnetic field of light, respectively. Subscripts I, R, and T correspond to the incident, reflected, and transmitted light, respectively.

**Figure 2-7.** Schematic representation of reflection and transmission in a three-phase model. Subscripts I, R, and T correspond to the incident, reflected, and transmitted light, respectively.

**Figure 2-8.** Schematic diagram of the apparatus for RAIRS, $Cs^+$ deposition, TPD, and Kelvin probe measurement.

**Figure 3-1**. (a) RAIR spectrum of a DCE film (29 ML thickness) that was sandwiched between $D_2O$ films (38 ML thickness). (b) The field difference spectrum, which is the absorbance difference between the field-on and field-off spectrum. The difference spectrum is shown at 3× magnification. The applied electric field across the DCE film was $1.5 \times 10^8$ . The temperature of sample preparation and spectral acquisition was 75 K. The inset shows the molecular structures of gauche- and trans-DCE.

**Figure 3-2**. (a) RAIR spectrum of a DCE film (30 ML) prepared at 55 K. (b) RAIR spectrum after heating the sample at 90 K. (c) A thermal difference spectrum obtained by subtracting spectrum (a) from (b).

**Figure 3-3**. Spectral analysis of the $CH_2$ wagging bands of DCE in the field difference spectrum (black line). The contributions of the trans-to-gauche conversion (red dashed line) and the reorientation of gauche conformer (blue dashed line) are shown.

**Figure 3-4**. Theoretical curve of relative absorbance change ($\Delta A/A_0$) versus average tilt angle ($\Delta\theta$) of permanent dipole of gauche-DCE. The curve for $G_{\parallel}$ band is shown in blue, and $G_{\perp}$ band, in red. The molecular dipole direction is indicated by a black arrow. The directions of transition dipole moments of $G_{\parallel}$ and $G_{\perp}$ vibrations are indicated by blue and red double-ended arrows, respectively. The experimental $\Delta A/A_0$ values are marked with dotted lines.

**Figure 3-5**. The field difference spectra for the $CH_2$ wagging bands of DCE samples at three temperatures (8, 50, and 90 K). The sample preparation and spectral acquisition were made at the same indicated temperature. The applied field strength was approximately $1 \times 10^8$ V $m^{-1}$.

**Figure 4-1.** RAIR spectra of various AA samples between 1900 $cm^{-1}$ and 1350 $cm^{-1}$. Eachsample was prepared on a Pt (111) surface at 70 K. (a) A pure AA film (25 ML) (b) A mixed AA-$NH_3$ film with an AA:$NH_3$ molar ratio of 1:20. (c) An "AA(top)/$NH_3$(bottom)" sample, with a structure of $D_2O$ (41 ML)/AA (25 ML)/$NH_3$ (12 ML)/$D_2O$ (41ML)/Pt(111).

**Figure 4-2.** (a) Changes in RAIR spectra as the thickness of the AA film on the $NH_3$ film increased. Spectra marked "x ML → y ML" show the absorbance change when the AA film thickness was changed from x ML to y ML. (b) Intensity changes of the ν(C=O) in AA and ν(CO) in $AA^-$ peaks according to AA film thickness.

**Figure 4-3.** (a) (Top) RAIR spectrum of an $NH_3$(top, 12 ML)/AA(bottom, 25 ML) layered film. (Bottom) The field-on minus field-off difference spectrum. The difference spectrum was magnified by a factor of ten. (b) Relative absorbance changes in the ν(CO) in $AA^-$ as a function of the applied electric field strength. To change the direction of the applied field, the stacking sequence of the AA and $NH_3$ films was reversed. The field directions are indicated as (+)$NH_3$/AA(–) and (+)AA/$NH_3$(–).

**Figure 4-4.** (a) (Top) RAIR spectrum and field difference spectrum of an $NH_3$(top, 12 ML)/FA(bottom, 19 ML) layered film at $F = 1.4 \times 10^8$ $Vm^{-1}$.

(Bottom) RAIR spectrum and field difference spectrum of an $NH_3$(top, 12 ML)/PA(bottom, 20 ML) layered film at F = $1.4 \times 10^8$ $Vm^{-1}$. The difference spectra were magnified by a factor of 4. (b) Relative absorbance changes in the ν(CO) peaks of $FA^-$, $AA^-$, and $PA^-$ as a function of applied field strength. The data for AA is identical to that shown in Figure 4-3(b).

**Figure 4-5.** Illustration of field-induced acid dissociation mechanisms. (a) Electrostatic mechanism. When the $OH^{\cdots}N$ hydrogen bond of the AA-$NH_3$ pair is properly oriented along the field direction, the field facilitates proton transfer from AA to $NH_3$ by electrostatically stabilizing the charged transition state and the product. (b) Reorientation mechanism. The field reorients the AA (or $NH_3$) molecule to provide the AA-$NH_3$ pair with a favorable geometry for spontaneous proton transfer. Note that the field direction is opposite to that of proton transfer via the electrostatic mechanism. The dipole moment of AA is indicated by $\mu_{AA}$.

**Figure 4-S1.** (Top) RAIR spectrum of a sandwiched 35 ML AA film. $D_2O$ (40 ML)/AA (35 ML)/$D_2O$ (40 ML)/Pt(111) ν(CO) in $AA^-$ is not shown, which indicates that AA molecule did not dissociate at the AA-D2O interface. (Bottom) Field difference spectra.

**Figure 4-S2.** RAIR spectrum of an $NH_3$(top, 12 ML)/AA(bottom, 25 ML)

layered film. ($D_2O$ (41 ML)/AA (25 ML)/$NH_3$ (12 ML)/$D_2O$ (41ML)/Pt(111)) (a) (Top) RAIR spectrum of the layered film in range of NH Stretching (Bottom) Field difference spectra. (b) (Top) RAIR spectrum of the layered film in range of NH wagging mode. (Bottom) Field difference spectra.

**Figure 4-S3.** (a) (Top) RAIR spectrum of an $NH_3$(top, 12 ML)/AA(bottom, 25 ML) layered film. (Bottom) The field-on minus field-off difference spectra. (b) (Top) RAIR spectrum of an AA(top, 25 ML)/$NH_3$(bottom, 12 ML) layered film. (Bottom) The field-on minus field-off difference spectra. The difference spectra were magnified by a factor of 5.

**Figure 4-S4.** (a) (Top) RAIR spectrum of an $NH_3$(top, 12 ML)/FA(bottom, 19 ML) layered film. (Bottom) The field-on minus field-off difference spectra. (b) (Top) RAIR spectrum of an $NH_3$(top, 12 ML)/PA(bottom, 20 ML) layered film. (Bottom) The field-on minus field-off difference spectra. The difference spectra were magnified by a factor of 5.

# Chapter I

# Introduction

Electric fields influence various physical and chemical phenomena in nature via the electrostatic interactions between the field and charges in molecules. Many researchers have studied the electric field effect to understand and control field-induced phenomena, such as the reduction/oxidation and reorientation of water on electrode surfaces, configuration changes in large biomolecules, and the field ionization of water molecules.[1-3] Traditionally, the electric field effect has been studied in electrochemical cells via electroanalytical methods, including voltammetry and amperometry. Although these studies have contributed greatly to our understanding of the electric field effect, many physical/chemical aspects remain unclear because of experimental limitations. Recently, various methods have been devised to generate strong electric fields and monitor physical/chemical changes under an electric field at the molecular scale.

In the chapter I-1, I briefly describe various experimental methods that are currently used to study field-induced phenomena, with a particular focus on the advantages and disadvantages of these methods. In the chapter I-2, an 'ice-film-capacitor method' developed by our group for studying the effect of applied electric fields on condensed-phase molecules is introduced.

## I-1. Experimental Methods for Studying the Electric Field Effect

The most common method of applying a strong electric field is the use of an electrochemical cell. In this method, an electric field exceeding $10^9$ V $m^{-1}$ is applied within the electrical double layer (EDL), which has a thickness of a few nanometers or less on the electrode surface. This strong field induces a variety of chemical reactions in the EDL. Despite their wide application, electrochemical cells have several challenges to be adopted for studying field-induced phenomena at the molecular scale. One of these challenges is the characterization of the electric field in the EDL. Indeed, although the characteristics of the electric field have been theoretically predicted, they have not yet been directly experimentally measured. Many researchers have attempted to measure the strength of an electric field in the EDL using vibrational Stark effect spectroscopy, X-ray photoelectron spectroscopy, and scanning tunneling microscopy.[4-6] Additionally, the physical/chemical changes in the EDL are difficult to detect because of the small thickness of the EDL. Recently, several surface-sensitive techniques have been employed to measure field-induced changes in the EDL, such as ambient pressure X-ray absorption spectroscopy, attenuated total reflectance spectroscopy, and sum frequency generation spectroscopy.[3, 7-8]

A charged-metal-plates method is one of the simplest approaches to generate a strong electric field with the field strength of up to $10^7$ V $m^{-1}$, which is determined by the applied voltage and the distance between plates in a homogeneous system. The orientation of a polar molecule can be controlled

under the electric field and the orientation dependence of reactions was analyzed in crossed molecular beam experiments.[9-10] Many groups combined this technique with spectroscopic methods using a sample cell consisting of sapphire windows coated with transparent metal layers. This method has been widely used to observe electric field effects such as Stark effects and the electrochromism of molecules in a condensed-phase.[11-13] The maximum strength, however, is not sufficient to induce various field-induced phenomena in a condensed-phase.

Scanning tunneling microscopy (STM) has been used to study the electric field effect near the metal surface. The STM tip can approach to the surface at an angstrom scale and the extremely strong electric field ($10^{10}$ V $m^{-1}$) can be generated between them. However, the effective field area is confined only near the tip, and the application of this method is limited to single molecule phenomena. The STM technique has been used to study the field-induced ionization, isomerization, and Diels-Alder reaction on a metal surface by measuring the tunneling current, STM images, and field-induced desorbed ions.[2, 14-15]

## I-2. Advantages of Ice Film Capacitor Method

We developed an 'ice-film-capacitor method' that could be suitable for studying electric field-induced phenomena by overcoming the disadvantages of previous experimental tools.[16] This method involves an ice film grown on a metal substrate in ultra-high vacuum (UHV), and the ice film is charged via

the deposition of low-energy $Cs^+$ ions on the surface. This charging can generate a $10^8$ V $m^{-1}$ electric field across the film, which is stronger than that achieved by conventional methods using charged metal plates. The field strength can be controlled by changing the amount of $Cs^+$ ions, and characterized using a Kelvin work-function probe and vibrational Stark effect methods. This ice-film-capacitor method has the ability to control the sample structure and composition in a clean vacuum environment and is compatible with the infrared (IR) spectroscopy method, thus enabling the direct monitoring of molecular changes under an applied electric field.

This thesis aims to understand field-induced isomerization and acid-dissociation by using the ice-film-capacitor method. In chapter II, the experimental methods used in the study are described. In particular, the ice-film-capacitor method is explained in detail. Chapter III presents the investigation of the conformational change of 1,2-dichloroethane under an external electric field by using IR spectroscopy. In chapter IV, the field-induced acid dissociation studied using the ice-film-capacitor method is discussed. The dissociation of acetic acid monitored by using IR spectroscopy and the mechanism of field-induced acid dissociation are also discussed.

## Reference


1. Fried, S. D.; Bagchi, S.; Boxer, S. G., *Science* **2014**, *346*, 1510.
2. Stuve, E. M., *Chem. Phys. Lett.* **2012**, *519*, 1.
3. Velasco-Velez, J.-J.; Wu, C. H.; Pascal, T. A.; Wan, L. F.; Guo, J.; Prendergast, D.; Salmeron, M., *Science* **2014**, *346*, 831.
4. Lambert, D. K., *Electrochim. Acta* **1996**, *41*, 623.
5. Favaro, M.; Jeong, B.; Ross, P. N.; Yano, J.; Hussain, Z.; Liu, Z.; Crumlin, E. J., *Nature communications* **2016**, *7*.
6. Woo, D.-H.; Yoo, J.-S.; Park, S.-M.; Jeon, I. C.; Kang, H., *Bull. Korean Chem. Soc* **2004**, *25*, 577.
7. Baldelli, S., *Acc. Chem. Res.* **2008**, *41*, 421.
8. Osawa, M.; Ataka, K.-i.; Yoshii, K.; Yotsuyanagi, T., *J. Electron. Spectrosc. Relat. Phenom.* **1993**, *64*, 371.
9. Loesch, H.; Remscheid, A., *J. Chem. Phys.* **1990**, *93*, 4779.
10. Beuhler Jr, R. J.; Bernstein, R. B., *J. Chem. Phys.* **1969**, *51*, 5305.
11. Bublitz, G. U.; Boxer, S. G., *Annu. Rev. Phys. Chem.* **1997**, *48*, 213.
12. Andrews, S. S.; Boxer, S. G., *J. Phys. Chem. A* **2000**, *104*, 11853.
13. Boxer, S. G., *J. Phys. Chem. B* **2009**, *113*, 2972.
14. Alemani, M.; Peters, M. V.; Hecht, S.; Rieder, K.-H.; Moresco, F.; Grill, L., *JACS* **2006**, *128*, 14446.
15. Aragonès, A. C.; Haworth, N. L.; Darwish, N.; Ciampi, S.; Bloomfield, N. J.; Wallace, G. G.; Diez-Perez, I.; Coote, M. L., *Nature* **2016**, *531*, 88.
16. Shin, S.; Kim, Y.; Moon, E.-s.; Lee, D. H.; Kang, H.; Kang, H., *J. Chem. Phys.* **2013**, *139*, 074201.

# Chapter II

# Method

## II-1. Ice Film Capacitor Method

Ice film capacitor method operates via the interfacial charging of cesium ions on an ice film surface.[1-2] The ice film was grown on a metal substrate surface by water vapor deposition inside an ultra-high vacuum (UHV) chamber. $Cs^+$ ions were sprayed onto the ice film surface with a low energy (< 20 eV) to prevent damage from ion impact. The same number of electrons was drawn at the metal-water interface, and this charging generates a voltage difference across the film. (Figure 2-1) Cesium ions do not penetrate into the interior of ice because they have a thermodynamic affinity for the ice surface.[1] The film voltage was measured using a Kelvin probe, which detected a contact potential difference (CPD) between the sample and the Kelvin probe tip. The difference in the film voltage (ΔCPD) before and after ion deposition indicated the film voltage developed by $Cs^+$ deposition. Various molecular films can be studied using the ice film capacitor method by sandwiching these films between two water layers.

The electric field in the sandwiched film can be determined using a parallel plate capacitor model. For homogeneous sample composition, the film voltage is given by

$$V_{film} = \frac{\sigma d}{\varepsilon_r \varepsilon_0} \quad \text{(eqation 2-1)}$$

where $\sigma$ is a charge density on the surface, $\varepsilon_0$ is the permittivity of vacuum, and $d$ and $\varepsilon_r$ are the thickness and the dielectric constant of the film, respectively. This model assumes that the surface densities of $Cs^+$ and electron are uniform. The field strength inside a film was determined by simply dividing ΔCPD with the film thickness. The measured film voltage was approximately 10 V and the film thickness was about $10^{-7}$ m; therefore, a $10^8$ $Vm^{-1}$ electric field was generated using the ice film capacitor method.

In case of a sandwiched film, the measured film voltage is the sum of voltages of a sample film and cover films,

$$V_{film} = V_{sample} + V_{cover} \qquad \text{(equation 2-2)}$$

and the strength of the electric field in the sample film is determined as

$$E_{sample} = \frac{V_{film}}{[d_{sample} + \frac{d_{cover}\varepsilon_{sample}}{\varepsilon_{cover}}]} \qquad \text{(equation 2-3)}$$

where $d_i$ and $\varepsilon_i$ are the thickness and dielectric constant of film $i$, respectively.

Figure 2-2 (a) shows ΔCPD values measured upon exposing the sample to $Cs^+$ ions. The $Cs^+$ beam energy was fixed at 20 eV during the exposure. It was observed that the film voltage increased linearly in the early stages of ion exposure (~ 5 min) and the increase in the film voltage gradually slowed down with increasing ion-exposure times. The slower increase of ΔCPD indicates that the developed film voltage reduced the sticking efficiency

of the incident $Cs^+$ ions to the film surface. The $Cs^+$ ion trajectories may bend near the charged film where an inhomogeneous field region is developed, thus the amount of $Cs^+$ ion reaching the film surface is decreased by the $Cs^+$ charging.

The bending of ion trajectories is also observed during $Cs^+$ current measurement. Figure 2-2 (b) shows the $Cs^+$ current of the sample based on the ion exposure time. The $Cs^+$ beam energy changed from 7 eV to 15 eV at specific moments, indicated by arrows in Figure 2-2 (b). The $Cs^+$ current gradually decreased at the static $Cs^+$ energy with increasing exposure time, and increased with increasing $Cs^+$ beam energy. A decrease in the ion current also supports the reduce of the sticking efficiency of the incident $Cs^+$ ions. When the energy of the $Cs^+$ beam is increased, the beam current sharply increases, because the kinetic energy of $Cs^+$ ions increases and $Cs^+$ ion arrive at the film surface more easily. Although we measured the "sample current" through a picoammeter connected to the metal substrate, it represented not only the ions arriving on the sample surface but also those reaching other parts of the sample holder. Because it was difficult to measure only the ions reaching the sample surface, we could not determine the exact amount of the charge accumulated on the film.

Figure 2-3 plots the maximum voltage across the ice film developed after the saturation of $Cs^+$ exposure at different beam energies (10–100 eV). The data point for 10 eV was measured after exposing the sample to $Cs^+$ ions at a constant beam energy of 10 eV from the beginning till the point of ion saturation. Then, the beam energy was increased to 20 eV; ion exposure was

continued on the same sample to the point of ion saturation, giving rise to the maximum film voltage with the 20 eV beam energy. Similar procedures were carried out to obtain the data at the beam energies of 50 and 100 eV.

Figure 2-3 shows that an increase in the beam energy beyond 50 eV was ineffective in increasing the film voltage. The maximum film voltage was 17.6 V at 50 eV. This saturation suggests that the charge-density saturation on the ice surface limits the highest field attainable in the sample. The surface density of $Cs^+$ ions can be estimated using the plate capacitor model (equation 2-1). The surface charge density is $\sigma \approx 5 \times 10^{-3}$ C $m^{-2}$ with $d = 6.5 \times 10^{-8}$ m and $\varepsilon_r \approx 2$ at a film voltage of 17.6 V. This value corresponds to a $Cs^+$ surface coverage of $3 \times 10^{16}$ ions $m^{-2}$, which is an enormously dense population of ions floating on the ice surface. Experiments with samples of different thicknesses showed approximately linear proportionality between the sample thickness and the maximum film voltage (not shown). These observations indicated that the maximum surface charge density was approximately the same for all samples. If interionic Coulomb repulsion is strong enough, it may be able to overcome the thermodynamic forces that hold $Cs^+$ ions on the surface. If this happens, additional $Cs^+$ ions will no longer accumulate on the surface and increase the film voltage, but will rather migrate to the interior of the ice.

In our experiment, the densities of $Cs^+$ ions and electrons were not uniform on the film surfaces, which may cause the fluctuation of field strength. The amount of fluctuation was determined by classical electrostatic calculation. The model film was assumed to be a 4000 $nm^2$ square plate film

(x, y) with a height (z) of 40 nm. (Figure 2-4) The width of the model film was reduced to that of the real ice film (~cm scale) to minimize the calculation time. The $Cs^+$ ions and electrons were treated as point charges, arranged periodically on the film surface (xy surface) with a charge density of $2.5 \times 10^{-3}$ $ML^{-1}$ ($\approx 2.5 \times 10^{16}$ ions $m^{-2}$).

The z-axis electric field at the position $r$ was determined as

$$E_z(r) = \sum_i \frac{q_i}{4\pi\varepsilon_0}\left[\frac{1}{(\boldsymbol{r}-\boldsymbol{r_i})^2}\right]_z \qquad \text{(equation 2-4)}$$

where $q_i$ and $\boldsymbol{r_i}$ are the charge and position of particle $i$, respectively.

Figure 2-5 shows the strength of electric field with a varying x position at a constant y position of 2000 nm. This calculation showed that the field fluctuation largely depends on the distance (z) from the charge. The electric field at z =0.8 nm shows a large fluctuation of electric field from $9 \times 10^7$ $Vm^{-1}$ to $1.2 \times 10^9$ $Vm^{-1}$, which means that the parallel plate capacitor method is not valid in this surface region. The field fluctuation decreases when the distance from the charge is increased, and the field strength approaches a constant value identical to that of the capacitor model. The field fluctuation is less than $1 \times 10^7$ $Vm^{-1}$ at z =4 nm. In the ice film capacitor method, the sample film was sandwiched by the water films (~10 nm). Therefore, the fluctuation of the electric field in the sample can be negligible, and the strength of the field can be determined using the parallel plate capacitor model.

## II-2. Reflection Absorption FT-IR Spectroscopy

Vibrational spectroscopy is a non–destructive tool that provides information about the molecular composition, structure, and interactions within a sample. It measures the vibrational energy level of molecules, which is usually in the infrared region. To study a thin film adsorbed on reflective surfaces under UHV conditions, reflectance absorption infrared spectroscopy (RAIRS) is commonly used.[3-6] RAIRS measurements are performed in grazing angle (84°) reflection geometry, and the intensity of reflected light is measured. Therefore, several optical effects should be considered to understand the IR spectrum of reflected light.

The reflection and transmission of light occur at the interface of two different types of matter because of their different refractive indexes. The Fresnel equation describes the relative amount of reflection at the interface of two different mediums. The amount of light is measured experimentally in the form of intensity, which is proportional to the square of the amplitude of electric field in light. *Reflectance* and *Fresnel reflection coefficient* are defined as the intensity and amplitude ratio between the electric field of the incident beam and that of the reflected beam, respectively.

In case of two-phase (Figure 2-6), *Fresnel reflection coefficients* are determined as

$$r_{12}^{s} = \frac{F_R^s}{F_I^s} = \frac{\tilde{n}_1 cos\theta_I - \tilde{n}_2 cos\theta_T}{\tilde{n}_1 cos\theta_I + \tilde{n}_2 cos\theta_T} \quad \text{(equation 2-5)}$$

$$r_{12}^{p} = \frac{F_R^p}{F_I^p} = \frac{\tilde{\varepsilon}_2 \tilde{n}_1 cos\theta_I - \tilde{\varepsilon}_1 \tilde{n}_2 cos\theta_T}{\tilde{\varepsilon}_2 \tilde{n}_1 cos\theta_I + \tilde{\varepsilon}_1 \tilde{n}_2 cos\theta_T} \quad \text{(equation 2-6)}$$

where $F_I^{s,p}$ is the amplitude of the electric field of the incident beam, $F_R^{s,p}$ is the amplitude of the electric field of the reflected beam, $\tilde{n}_i$ is the complex refractive index of medium i, $\tilde{\varepsilon}_i$ is the complex dielectric constant of medium $i$, $\theta_I$ is the incident angle, and $\theta_T$ is the refraction angle. The relationship between *Reflectance* and the *Fresnel reflection coefficient* is,

$$R_{12}^{s,p} = \left|r_{12}^{s,p}\right|^2 \quad \text{(equation 2-7)}$$

In RAIRS, the injected light passes through a vacuum, a film, and a metal phase. In the case of the three-phase model[7] (Figure 2-7), the *Fresnel reflection coefficients* are

$$r_{123}^{s} = \frac{r_{12}^{s}+r_{23}^{s}\exp(-2i\beta)}{1+r_{12}^{s}r_{23}^{s}\exp(-2i\beta)} \quad \text{(equation 2-8)}$$

$$r_{123}^{p} = \frac{r_{12}^{p}+r_{23}^{p}\exp(-2i\beta)}{1+r_{12}^{p}r_{23}^{p}\exp(-2i\beta)} \quad \text{(equation 2-9)}$$

where

$$\beta = \frac{2\pi i\tilde{n}_2 d\cos\theta_I}{\lambda} \quad \text{(equation 2-10)}$$

is the change in phase of the beam during one traversal of the thin film, $\lambda$ is the wavenumber of light in a vacuum, $d$ is the thickness of the thin film and $\theta_I$ is the incident angle. Subscripts 1, 2, and 3 correspond to the vacuum, thin layer, and metal substrate, respectively.

In this thesis, *reflectance* is expressed as *absorbance* or *reflectance-absorbance*, $A$, defined as

$$A = -log\frac{R}{R_0} \quad \text{(equation 2-11)}$$

, where $R_0$ is the *reflectance* without the thin film sample and $R$ is the *reflectance* with the thin film sample.

The sample film is much thinner than the wavelength of the IR beam ($d \ll \lambda$); therefore, *Fresnel reflection coefficients* in equations 2-8 and 2-9 can be approximated[7] to

$$r_{123}^{s,p} \approx \frac{r_{12}^{s,p} + r_{23}^{s,p}(1-2i\beta)}{1 + r_{12}^{s,p} r_{23}^{s,p}(1-2i\beta)} \quad \text{(equation 2-12)}$$

, and *absorbance* (or *reflectance-absorbance*) can be approximated as

$$A^s = -log\frac{R^s}{R_0^s} \approx -\log(1 + 8\pi d cos\varphi_1 v \mathrm{Im}(\tilde{\varepsilon}_2)) \approx$$

$$[8\pi cos\theta_1 v \mathrm{Im}(\tilde{\varepsilon}_2)]\mathrm{d} \quad \text{(equation 2-13)}$$

$$A^p = -log\frac{R^p}{R_0^p} \approx -\log(1 + 8\pi d sin\varphi_1 tan\varphi_1 v \mathrm{Im}(\frac{1}{\tilde{\varepsilon}_2})) \approx$$

$$[8\pi sin\theta_1 tan\theta_1 v \mathrm{Im}(\frac{1}{\tilde{\varepsilon}_2})]d \quad \text{(equation 2-14)}$$

According to equation 2-14, *absorbance* in RAIRS is directly proportional to the film thickness, which means that RAIRS can be used for quantitative analysis. The linearity between *absorbance* and the film thickness is not valid in the case of a thick film. The range of the application of the linear approximation was checked by measuring *absorbance* according to the film thickness, and the results showed that this approximation is valid for films thinner than 100 ML in the case of a $H_2O$ film.

The *absorbance* of the s-polarized light vanishes, while that of p-polarized light survives at the grazing angle as shown in equations 2-13 and 2-14. The orientation change of a molecule can be studied using RAIRS with this surface selection rule.[8-9] The absorbance depends on the angle between the transition dipole moment and the polarization vector of the electric field in light, which can be explained quantitatively by using quantum electrodynamics.[10] In this thesis, I will describe the theory of absorption in a simple way by using a two-state model based on the semi-classical electrodynamics and perturbation theory.[11]

I assumed that a system can be described by the sum of a molecular Hamiltonian and a dipole-electric field interaction Hamiltonian.

$$\hat{H} = \hat{H}_{mol} + \hat{H}'(t) \qquad \text{(equation 2-15)}$$

The molecular Hamiltonian is a time-independent Hamiltonian of the system in the absence of radiation, and the solution of this molecular Hamiltonian is expressed as

$$\hat{H}_{mol}\psi_n = E_n\psi_n \quad \text{(n=1 or 2)} \qquad \text{(equation 2-16)}$$

where $\psi_n$ and $E_n$ are a wave function and energy of the $n^{th}$ state, respectively, and subscripts 1 and 2 correspond to the ground state and an excited state in the vibrational mode, respectively.

The dipole-electric field potential Hamiltonian is described as

$$\hat{H}'(t) = -\vec{\mu} \cdot \vec{p} F_0 \cos(\omega t) \qquad \text{(equation 2-17)}$$

where $\vec{\mu}$ is the dipole moment of a molecule, and $\vec{p}$, $F_0$, and $\omega$ are the polarization vector, amplitude, and angular frequency of the electric field, respectively.

The evolution of the system over time is described using a time-dependent Schrödinger equation and the wave function is described as the linear combination of the two wave functions.

$$\widehat{H}\Psi(\vec{r},t) = i\hbar\frac{\partial}{\partial t}\Psi(\vec{r},t) \quad \text{(equation 2-18)}$$

$$\Psi(\vec{r},t) = a_1(t)\psi_1(\vec{r})e^{-\frac{iE_1t}{\hbar}} + a_2(t)\psi_2(\vec{r})e^{-\frac{iE_2t}{\hbar}} \quad \text{(equation 2-19)}$$

where $a_n$ is an expansion coefficient of the nth state.

The dipole-electric field potential energy is much weaker than the molecular potential energy, and the total Hamiltonian can be solved using the perturbation approximation. Almost vibration state is in ground state, and only a small amount of the population is excited $(a_1(t) \approx 1)$ because of the weak intensity of light in FT-IR spectroscopy.

Under these conditions, the coefficient of the excited state wavefunction can be approximated as

$$a_2(t) \approx \frac{F_0}{2\hbar}\left[\frac{e^{-i\left(\omega+\frac{E_1-E_2}{\hbar}\right)/t}-1}{\left(\omega+\frac{E_1-E_2}{\hbar}\right)}\right]|\vec{\mu}_{12}||\vec{p}|\cos\theta \quad \text{(equation 2-20)}$$

where

$$\vec{\mu}_{12} = \langle\psi_1(\vec{r})|\vec{\mu}|\psi_2(\vec{r})\rangle \quad \text{(equation 2-21)}$$

is a transition dipole moment between states 1 and 2, and $\theta$ is the angle between the transition dipole moment and the polarization vector of the electric field.

The amount of absorption is proportional to the existence probability of the excited state. Therefore, an absorbance is proportional to the cosine square of the angle between the transition dipole moment and the polarization vector of the electric field.

$$A \propto |a_2(t)|^2 \propto \cos^2\theta \qquad \text{(equation 2-22)}$$

When an external electric field is applied to a thin film using the ice film capacitor method, the direction of the applied electric field is equal to the direction of electric field in p-polarized light. Polar molecules in the film can reorient such that a dipole of the molecules becomes parallel to the external field. By this reorientation, absorbance of vibrational modes increases or decreases according to the angle between the permanent dipole and the transitional dipole moment of the vibrational mode, and thus, the amount of reorientation can be estimated from the absorbance change.[8]

## II-3. Instruments

All the experiments were conducted in an ultra-high vacuum (UHV) chamber, equipped with instrumentation for reflection absorption infrared spectroscopy (RAIRS), temperature-programmed desorption (TPD) mass spectrometry, and work function measurements (Figure 2-8). The UHV was maintained by a

turbomolecular pump (Leybold), which is backed by a rotary vane pump (Edwards). The UHV chamber was maintained with a background pressure below $1 \times 10^{-10}$ Torr, and the pressure was monitored by an ion gauge (Granville-Philips) with a tungsten filament.

A molecular film was deposited on a Pt(111) single crystal surface (MaTeck) maintained at a low temperature (60-120 K) inside the UHV chamber. The Pt(111) surface was cleaned using sputtering and annealing procedures, and its cleanliness was verified from the TPD profile of the $H_2O$ monolayer formed on the surface.[12] The temperature of the Pt(111) crystal was variable in the range of 70−1200 K and was monitored with a Kapton coated N-type thermocouple wire (Kurt J. Lesker) attached to the crystal. The sample was cooled by a He-recycled refrigerator (CTI) and a liquid nitrogen container. Resistive heating was performed by loading an electric current on Ta heating wires from a DC power supply (Daedo Electronics) with a computation control through a temperature control system (Eurotherm) and LabVIEW.

Liquid samples were purified using freeze−vacuum−thaw cycles. The purity of the samples was checked by introducing the vapors of the samples into the chamber through a leak valve (Agilent) and analyzing it with a quadrupole mass spectrometer (Exterl). The vapors of samples were guided close to the Pt(111) substrate surface using a tube doser (home-made) or a backfilling method. The thicknesses of the molecular films were estimated from TPD measurements.

RAIRS measurements were performed at a grazing angle (84°)

reflection geometry using a Fourier-transform infrared (FTIR) spectrometer (PerkinElmer) with a mercury−cadmium telluride detector (InfraRed Associates). The IR beam came out through an external beam port in the spectrometer after passing an interferometer. The beam was focused by a flat mirror and a parabolic mirror, and then the beam was linearly p-polarized using a wire grid polarizer (Edmund Optics). The IR beam came into the chamber through a ZeSe viewport and came out after the reflection on the Pt surface. The beam was then sent to the MCT detector by toroidal mirror focusing. The beam path outside the UHV chamber was purged with dry nitrogen gas to minimize the absorption of $CO_2$ and $H_2O$ molecules in air. The baseline of the RAIR spectra was obtained from a clean Pt (111) surface before film preparation at a fixed position and temperature. RAIR spectra were averaged 256 times at a spectral resolution of 4 $cm^{-1}$ and the noise level of the IR spectrum was reduced to less than $5\times10^{-5}$ Abs under these conditions.

The deposition of low-energy $Cs^+$ ions was performed using a low energy alkali ion gun (Kimball Physics). The sample was fixed in position for RAIRS during the $Cs^+$ deposition. The beam current of $Cs^+$ was measured through a picoamperemeter (Keithley), which was connected to the Pt substrate. The $Cs^+$ beam was dispersed to deposit $Cs^+$ ion uniformly on an ice surface. The $Cs^+$ charging voltage was monitored by a Kelvin work-function probe (McAllister). The gold-coated Kelvin probe tip was approached to the sample by a linear translator. The distance between the tip and the sample was determined by the gradient of a capacitance current. The vibrational frequency of the tip was chosen as 110 Hz to avoid the resonance frequency of our system.

## Reference


1. Tsekouras, A. A.; Iedema, M. J.; Cowin, J. P., *Phys. Rev. Lett.* **1998**, *80*, 5798.
2. Shin, S.; Kim, Y.; Moon, E.-s.; Lee, D. H.; Kang, H.; Kang, H., *J. Chem. Phys.* **2013**, *139*, 074201.
3. Ayotte, P.; Marchand, P.; Daschbach, J. L.; Smith, R. S.; Kay, B. D., *J. Phys. Chem. A* **2011**, *115*, 6002.
4. Haq, S.; Clay, C.; Darling, G. R.; Zimbitas, G.; Hodgson, A., *Physical Review B* **2006**, *73*.
5. Moon, E.-s.; Kim, Y.; Shin, S.; Kang, H., *Phys. Rev. Lett.* **2012**, *108*, 226103.
6. Kim, Y.; Moon, E. S.; Shin, S.; Kang, H., *Angew. Chem. Int. Ed.* **2012**, *51*, 12806.
7. McIntyre, J.; Aspnes, D., *Surf. Sci.* **1971**, *24*, 417.
8. Shin, S.; Kim, Y.; Kang, H.; Kang, H., *J. Phys. Chem. C* **2015**, *119*, 15588.
9. Park, Y.; Kang, H.; Kang, H., *Angew. Chem. Int. Ed.* **2017**, *56*, 1046.
10. Craig, D. P.; Thirunamachandran, T.; Academic Press: London, 1984.
11. Levine, I. N.; Prentice Hall, 2000.
12. Haq, S.; Harnett, J.; Hodgson, A., *Surf. Sci.* **2002**, *505*, 171.

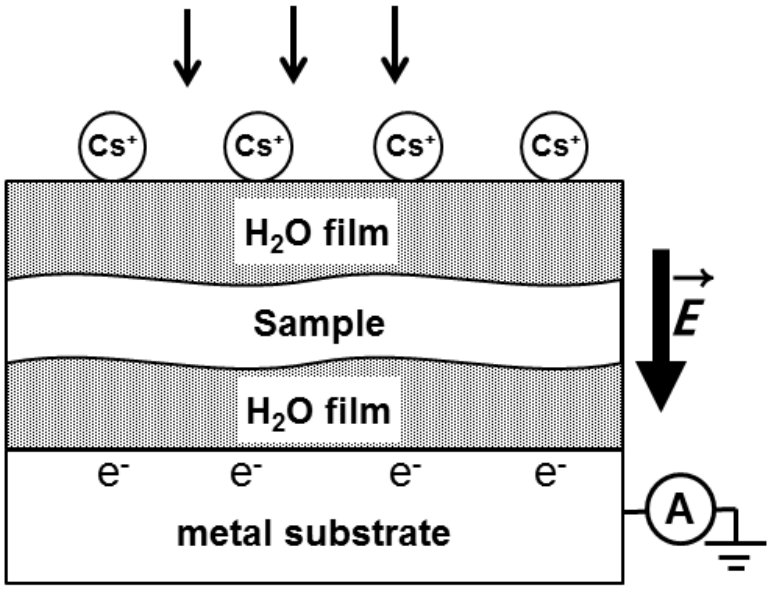


**Figure 2-1.** Schematic figure of an ice film capacitor. An ice film grown on a metal surface is charged by the deposition of $Cs^+$ ions onto the ice surface. Ion current is read by a picoamperemeter (A) connected to the metal substrate.

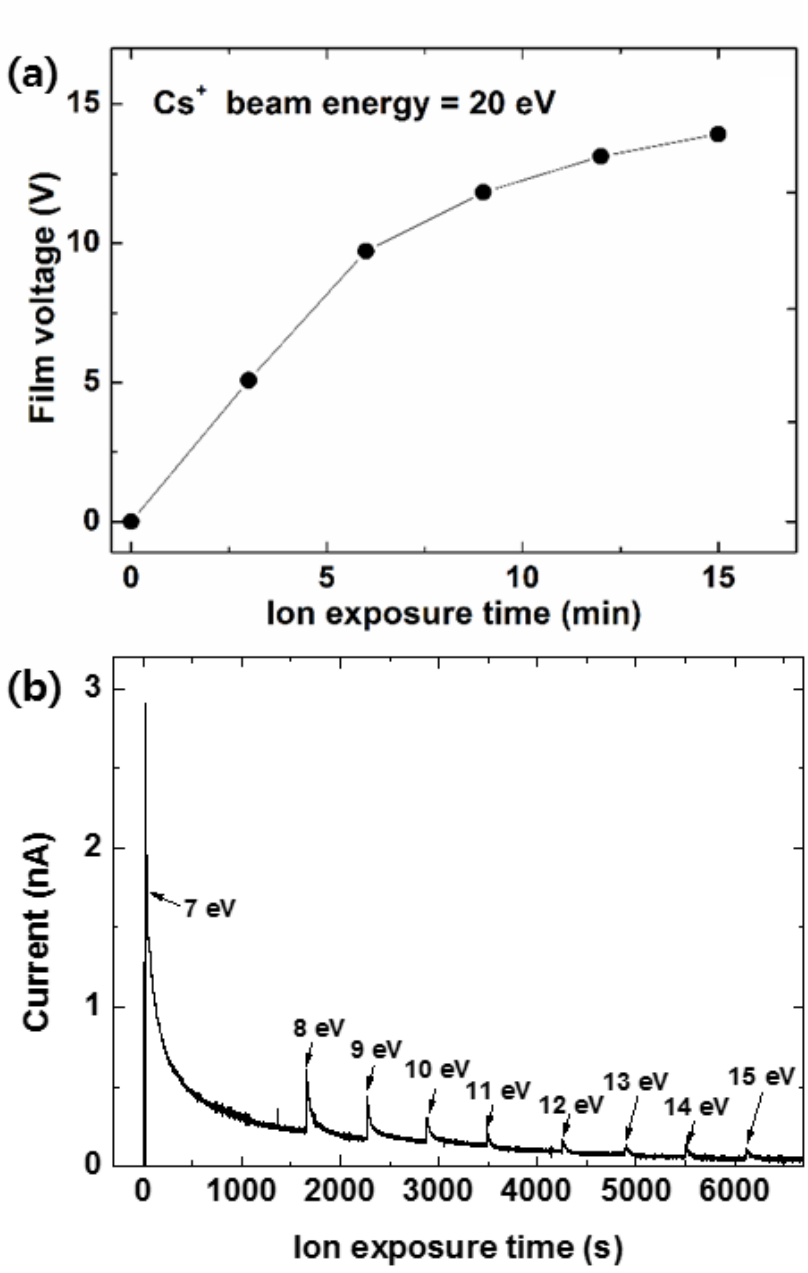


**Figure 2-2.** (a) Film voltages at varying an ion exposure times at a beam energy of 20 eV. The sample structure was $H_2O$ (20.1 nm)/acetonitrile (19.0 nm)/$H_2O$ (25.8 nm)/Ru (0001); (b) $Cs^+$ current depending on the ion exposure

time. The $Cs^+$ beam energy was changed from 7 eV to 15 eV. The exact times when the beam energy is changed are indicated by arrows.

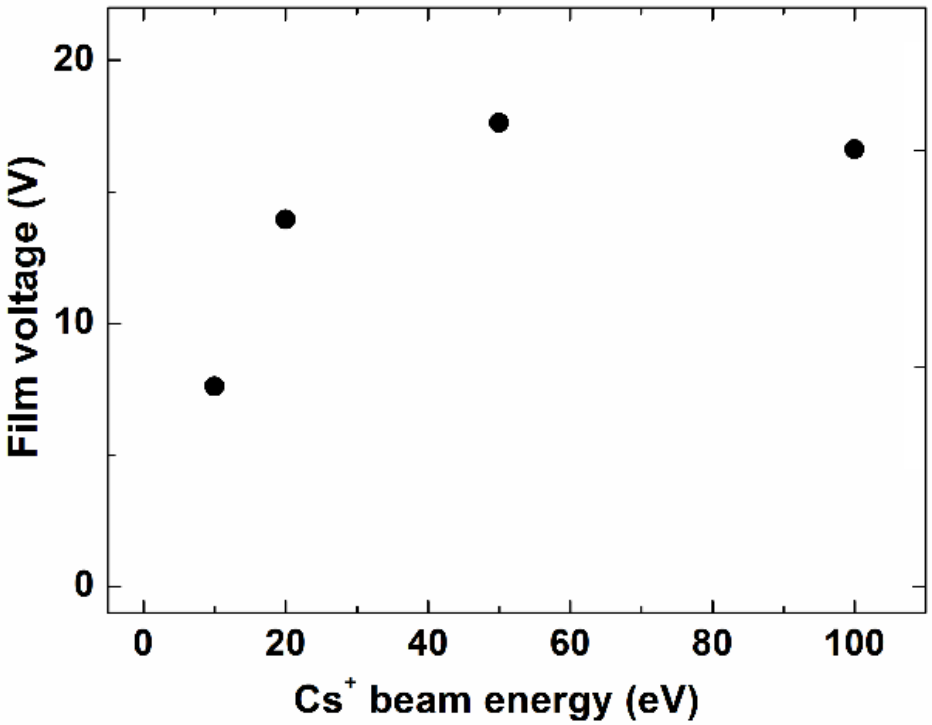


**Figure 2-3.** Maximum film voltages attained after ion-exposure saturation at different beam energies. The sample structure was $H_2O$ (20.1 nm)/acetonitrile (19.0 nm)/$H_2O$ (25.8 nm)/Ru (0001)

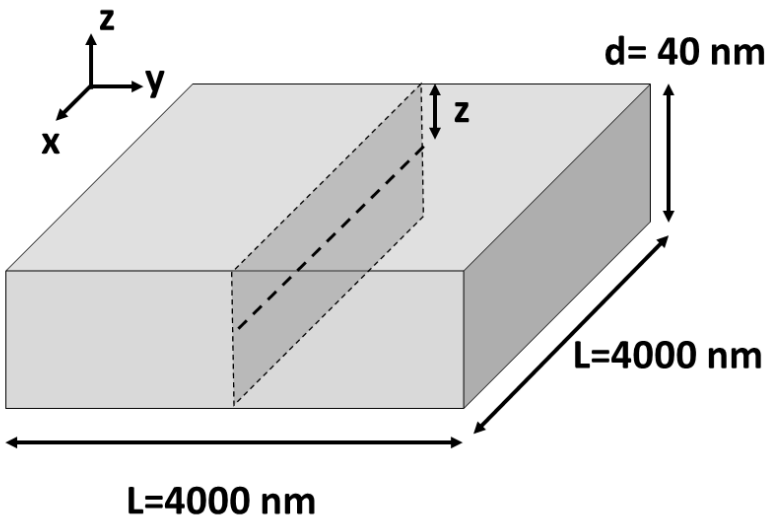


**Figure 2-4.** Dimensions of a plate capacitor model supporting a 4000 $nm^2$ plate film (x, y) with a height (z) of 40 nm.

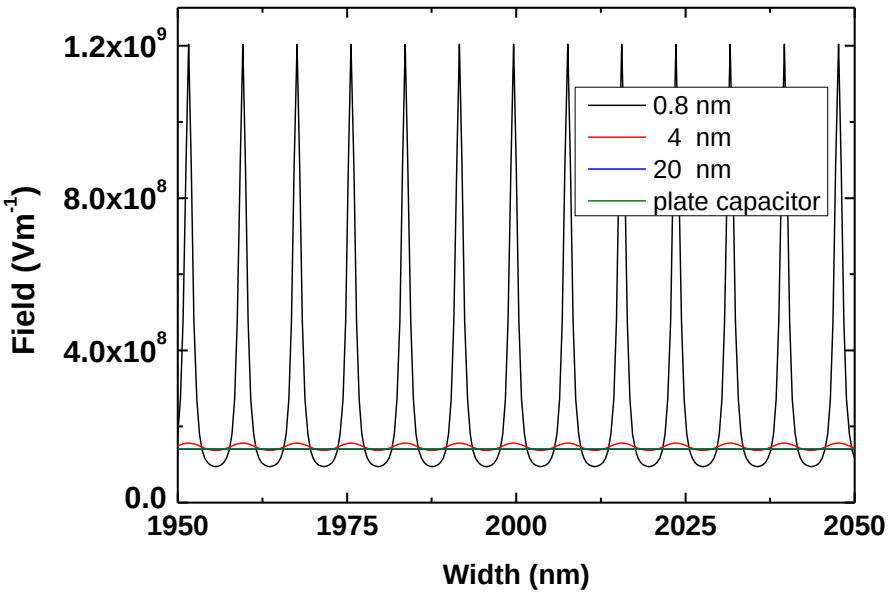


**Figure 2-5.** Strength of electric field at x positions from 1950 nm to 2050 nm at a constant y position of 2000 nm. The strength at z=0.8, 4, and 20 nm is expressed by black, red, and blue lines, respectively. The green line indicates the field strength expected from the plate capacitor model.

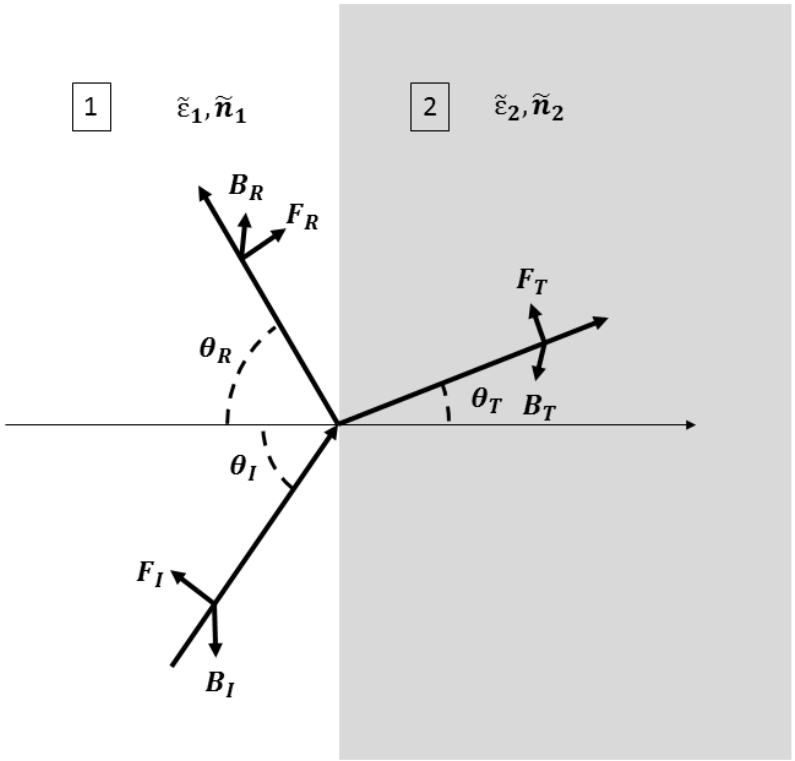


**Figure 2-6.** Schematic representation of the reflection and transmission at the interface between phases 1 and 2. **F** and **B** indicate the electric and magnetic field of light, respectively. Subscripts I, R, and T correspond to the incident, reflected, and transmitted light, respectively.

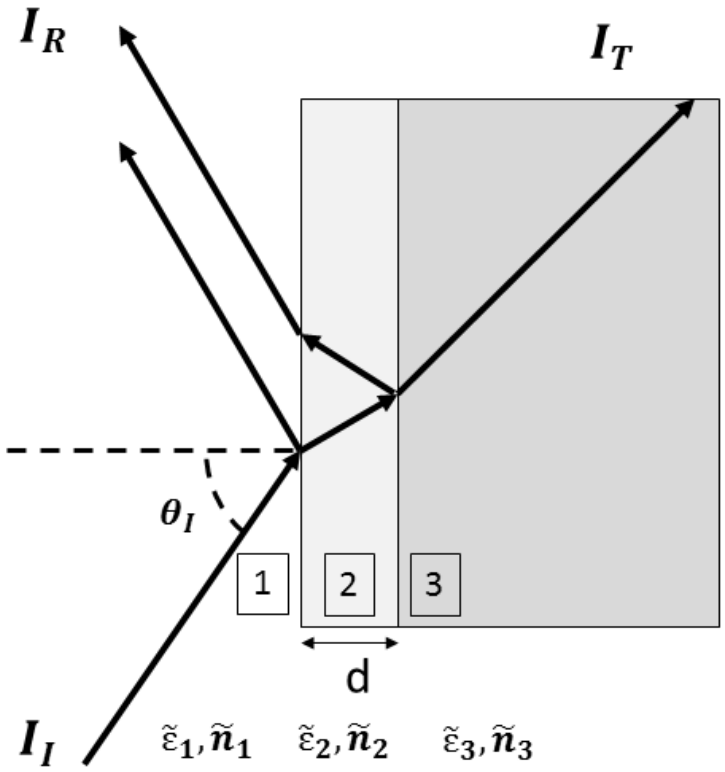


**Figure 2-7.** Schematic representation of reflection and transmission in a three-phase model. Subscripts I, R, and T correspond to the incident, reflected, and transmitted light, respectively.

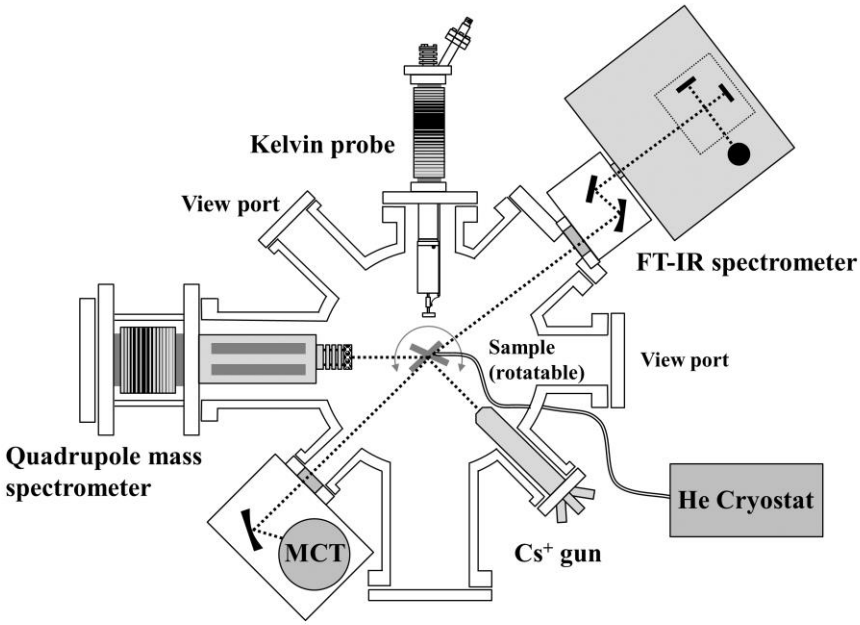


**Figure 2-8.** Schematic diagram of the apparatus for RAIRS, $Cs^+$ deposition, TPD, and Kelvin probe measurement.

# Chapter III

# Electric Field-Induced Conformational Changes of 1,2-Dichloroethane in Frozen Films

## Abstract

We studied how an externally applied electric field affects the conformation and orientation of 1,2-dichloroethane (DCE) in frozen molecular solid. An electric field in the order of $10^8$ V $m^{-1}$ was applied across the sample by means of interfacial charging of $Cs^+$ ions. Reflection absorption infrared spectroscopy (RAIRS) was used to monitor the gauche/trans conversion and reorientation of DCE molecules caused by electrostatic interaction with the field. Trans-DCE molecules were converted to gauche conformers via internal C-C rotation with the conversion efficiency of 24% at the field strength of 1.5 × $10^8$ V $m^{-1}$ at temperature 75 K. Gauche-DCE molecules were reoriented along the field by an average tilt angle of 36° under the same condition. These field-induced molecular changes were prohibited at 8 K and visible above 50 K. Therefore, both electrostatic and thermal energies were needed to induce molecular transformations in the metastable solid by overcoming the kinetic barrier. The study suggests the possibility of controlling molecular conformation and orientation of condensed molecular solid by applying an

external electric field whose magnitude is comparable to that of intermolecular electric fields.

## III-1. Introduction

The structural flexibility of molecules plays an important role in chemical and biological phenomena,[1-2] and a large amount of research effort has been given to study the conformational changes of molecules affected by environmental conditions such as pressure,[3] temperature,[4] and solvent.[5] Electric field is an important underlying force that influences molecular conformation in condensed phase via electrostatic intermolecular interactions. Numerous studies have been reported that examine the effect of electric field on molecular conformation, which range from the studies of biomolecular functions such as the configurational change of a potassium ion channel in response to the membrane potential,[6-7] to the structural changes of small flexible molecules under electric fields that are applied by various ingenious methods in different environments,[8-13] only to name a few.

The conformational change of 1,2-dichloroethane (DCE) under the influence of external electric field was first studied by Hamaguchi and coworkers.[11-13] By using infrared electroabsorption spectroscopy based on the phase-sensitive detection method coupled with an applied AC field, they detected a small change (~0.01 %) in the ratio of gauche and trans conformers in a liquid sample in equilibrium with the field of strength ~$10^7$ V $m^{-1}$.[11-12] They estimated that the gauche/trans ratio in liquid DCE at room temperature is 1.4 $\pm$ 0.2 and their free energy difference is 0.9 $\pm$ 0.4 kJ $mol^{-1}$.The observed conformational change was very small because the electrostatic energy difference of two conformers due to the dipole-field interaction (~0.1 kJ $mol^{-1}$ at ~$10^7$ V $m^{-1}$) was smaller than their free energy difference in the

liquid phase.[12, 14] Apparently, a much stronger field is needed to increase the conformational change of molecules to the level of "brute force" control using the field. Also, it is desirable that the applied field is in a DC mode and accurately measurable. Recently, Shin et al.[15] reported the ice film capacitor method, which can apply a DC electric field in the order of $10^8$ V $m^{-1}$ across a frozen molecular sample inside a vacuum chamber.[16-18] The method operates on the principle of charging a solid water surface with floating $Cs^+$ ions.[15] We use this method to study the conformational and orientational changes of DCE in a frozen molecular solid.

## III-2. Experimental Methods

Experiments were performed in an ultra-high vacuum (UHV) surface analysis chamber equipped with a low-energy $Cs^+$ ion gun, Kelvin work-function probe, Fourier transform infrared (FT-IR) spectrometer, and quadrupole mass spectrometer (QMS).[16] A frozen molecular film of DCE was prepared on a cold Pt(111) substrate surface via vapor deposition inside the UHV chamber. The Pt(111) surface was cleaned by $Ar^+$ sputtering and annealing procedures, and its cleanliness was verified from the temperature programmed desorption (TPD) profile of a $D_2O$ monolayer formed on the surface.[19] The temperature of the Pt(111) crystal was varied in the range 8−1200 K and was monitored using a N-type thermocouple wire attached to the crystal.

DCE and $D_2O$ liquids were purified using a freeze-vacuum-thaw cycling method. The purity of the samples was checked by introducing the

sample vapor into the chamber through a leak valve and analyzing it with a QMS. The DCE vapor was guided to the cold surface of a Pt(111) substrate using a tube doser and was deposited at a slower rate than 0.1 monolayer per second (ML $s^{-1}$). The $D_2O$ vapor was deposited using a backfilling method at 0.08 ML $s^{-1}$. The thicknesses of the molecular films were determined from TPD measurements. The thickness of the DCE film was estimated using the unit cell volume of a DCE crystal.[4] In this paper, the film thicknesses are expressed in units of ML, where 1 ML represents $1.9 \times 10^{14}$ molecules $cm^{-2}$ for DCE and $1.1 \times 10^{15}$ molecules $cm^{-2}$ for $D_2O$.

An electric field was applied across the samples using the ice film capacitor method[15], in which the ice film surface was charged positively with $Cs^+$ ions and the Pt substrate surface was charged negatively with electrons. The electric field strength ($F$) inside the ice film can be calculated from the relationship $F = V/d = \sigma/\varepsilon_r\varepsilon_o$, where $V$ is the voltage across the film, $d$ is the film thickness, $\sigma$ is the surface density of $Cs^+$ ions, $\varepsilon_r$ is the relative permittivity of the film, and $\varepsilon_o$ is the vacuum permittivity. The voltage across the film was measured using a Kelvin probe. In the present experiment, the sample was composed of multiple stacks of DCE and $D_2O$ films. In this case, the electric field strength within the DCE film can be expressed as

$$F(\mathrm{DCE}) = \Delta\mathrm{CPD}/[d(\mathrm{DCE}) + \frac{d(\mathrm{D_2O})\varepsilon_r(\mathrm{DCE})}{\varepsilon_r(\mathrm{D_2O})}$$

where $\Delta$CPD is the voltage across the whole film, $d(D_2O)$ and $d$(DCE) are the thicknesses of $D_2O$ and DCE films, respectively, and $\varepsilon_r(D_2O)$ and $\varepsilon_r$(DCE) are

dielectric constants. Because $\varepsilon_r$ for solid DCE is unknown, we estimated $\varepsilon_r$(DCE) using the Clausius-Mossotti relation,

$$\frac{\varepsilon_r(\mathrm{DCE})-1}{\varepsilon_r(\mathrm{DCE})+2} = \frac{N(\mathrm{DCE})\alpha(\mathrm{DCE})}{3\varepsilon_0}$$

where $\alpha(\mathrm{DCE})$ is a polarizability of DCE,[5] and $N(\mathrm{DCE})$ is a number density of DCE molecule. The dielectric constant of a $D_2O$ film was also estimated using the same relation as 1.6, which is similar with a previous reported value for a frozen water film ($\varepsilon_r$=2).[20]

Reflection absorption infrared spectroscopy (RAIRS) measurements were performed at a grazing angle of 84° using an FTIR spectrometer equipped with a mercury cadmium telluride detector. The beam path outside the UHV chamber was purged with dry nitrogen gas to minimize absorption by $CO_2$ and $H_2O$ in the air. The baseline for the RAIR spectra was obtained on a clean Pt(111) surface at the same position and temperature as that used for DCE samples. RAIR spectra were scanned 256 times at a spectral resolution of 4 $cm^{-1}$, and the noise level of IR spectra was lower than $5 \times 10^{-5}$ Abs under these conditions.

## III-3. Results and Discussion

We prepared a sample composed of a frozen DCE film sandwiched between two $D_2O$ films by vapor deposition on a Pt(111) substrate at 75 K. The $D_2O$ films were used as a spacer layer layers that prevent direct contact of DCE

with $Cs^+$ ions or a Pt surface. The RAIR spectrum of this sample is shown in Figure 3-1(a). DCE has two different conformers in local energy minima, named gauche and trans (also called anti) conformers depending on the relative positions of Cl atoms (see inset in Figure 3-1). The RAIRS features are assigned to vibrational bands of these conformers based on the IR spectral information obtained for liquid DCE samples.[21] To facilitate discussions to follow, we mark the vibrational bands of trans-DCE as T and those of gauche-DCE as G. The gauche-DCE bands can be classified further into $G_{\parallel}$ and $G_{\perp}$, depending on whether the direction of the transition dipole moment is parallel or perpendicular to the permanent dipole of gauche-DCE. The two peaks appearing at 1461 $cm^{-1}$ (labeled T) and 1433 $cm^{-1}$ (labeled G) are the $CH_2$ scissoring modes of trans- and gauche-DCE, respectively. The peaks at 1320 $cm^{-1}$ ($G_{\parallel}$) and 1280 $cm^{-1}$ ($G_{\perp}$) are the symmetric and asymmetric $CH_2$ wagging modes of gauche-DCE, and the peak at 1230 $cm^{-1}$ (T) is the $CH_2$ wagging mode of trans-DCE. The peaks at 948 $cm^{-1}$ ($G_{\parallel}$) and 890 $cm^{-1}$ ($G_{\perp}$) are the $CH_2$ rocking modes of gauche-DCE. The broad absorption around 1200 $cm^{-1}$ is assigned to $D_2O$ bending vibrations.

We applied an electric field across the sample using the method described in Section II. The absorbance difference of the spectra measured with the field on and off, called the field difference spectrum, is shown in Figure 3-1(b). The difference spectrum shows that the applied field decreased the trans-DCE bands while it increased the gauche-DCE bands. These changes indicate trans-to-gauche conversion of DCE molecules by the applied field.

In addition, the gauche-DCE bands exhibited different degrees of the intensity increase depending on the direction of transition dipole moment of vibrational mode. For example, the sym-$CH_2$ rocking band ($G_{\parallel}$) exhibited an increase of 45%, whereas the asym-$CH_2$ rocking band ($G_{\perp}$) increased only by 10%. Similar behaviors were observed for the symmetric ($G_{\parallel}$) and asymmetric $CH_2$ wagging ($G_{\perp}$) bands. Because RAIRS detects vibrational modes that have transition dipole moment component parallel to the p-polarization of light,[2, 16] which is also the direction of the applied field in the present experimental setup, the observed changes of vibrational band intensities indicate reorientation of gauche-DCE molecules toward the field direction. If the molecular dipole of gauche-DCE is reoriented along the field by electrostatic interaction, then the $G_{\parallel}$ bands will increase because their transition dipole moments become more aligned along the direction of p-polarization, whereas the $G_{\perp}$ bands will decrease. The observed spectral intensity changes indicate that the trans-to-gauche conversion and the molecular reorientation both occur. The net effect of two concurrent processes is that the $G_{\perp}$ bands increase by a smaller degree than the $G_{\parallel}$ bands.

The spectral changes due to the trans-to-gauche conversion and the molecular reorientation are analyzed as follows. To deconvolute the spectra, reference spectra for separate events are needed. For this purpose, we examined the conformational change of DCE molecules taking place in the absence of applied field just by sample heating. The initial sample was prepared at 55 K, and then it was heated at 90 K. RAIR spectra were measured

before and after the sample heating, shown in Figure 3-2. The absorbance difference of two spectra, called the thermal difference spectrum, is also shown.

The thermal difference spectrum shows a decrease of the trans conformer bands and an increase of the gauche conformer bands, which indicates the conversion from trans to gauche conformer upon the sample heating. This behavior is consistent with the lower free energy of the gauche conformer in a condensed phase due to intermolecular dipole-dipole interactions.[14] Note that heating the sample in the absence of external field does not cause dipolar polarization of the sample. Therefore, the thermal difference spectrum reflects one-to-one conversion from trans to gauche conformer, and can be used as a reference spectrum for this process. When the heated sample was cooled back to 55 K, the band intensities were not restored back to the preheated state. The irreversibility means that the trans/gauche population ratio in the sample was not in thermal equilibrium, which is consistent with the metastable nature of frozen molecular films.[22]

The field difference spectrum is analyzed by separating the effects of the trans-to-gauche conversion and the reorientation of gauche-DCE. Figure 3-3 highlights the $CH_2$ wagging band region of the field difference spectrum shown in Figure 3-1(b). The decreased absorbance at 1230 $cm^{-1}$, which is the $CH_2$ wagging band of trans-DCE, quantitatively represents the amount of trans-to-gauche conversion in the sample. This absorbance change is independent of the reorientation of gauche-DCE. The intensity of this band decreased by 24% at the field strength of $1.5 \times 10^8$ $Vm^{-1}$ compared to the zero-

field intensity, shown in Figure 3-1(a), which indicates that 24% of trans conformers were converted to gauche conformers via C-C bond rotation under the field.

The gauche conformers created by trans-to-gauche conversion contribute to increase the intensities of the $G_{\parallel}$ (1320 $cm^{-1}$) and $G_{\perp}$ (1280 $cm^{-1}$) bands. This increased portion can be predicted using the intensity changes in the thermal difference spectrum (Figure 3-2c) as a reference. For this, the thermal difference spectrum is fitted to the field difference spectrum by rescaling its absorbance such that the T band (1230 $cm^{-1}$) absorbance is matched for two spectra, which means that the lost amount of trans-DCE is equalized for two samples. The fitted thermal difference spectrum is indicated by a red dashed line in Figure 3-3. It shows the amount of increase of $G_{\parallel}$ and $G_{\perp}$ bands expected from the trans-to-gauche conversion.

The spectral change associated with the reorientation of gauche-DCE can be estimated by subtracting the contribution of the trans-to-gauche conversion (red dashed line) from the field difference spectrum. The subtracted spectrum, depicted by a blue dashed line in Figure 3-3, indicates the reorientation of gauche conformers. This spectrum can be used to estimate the degree of the field-induced reorientation of gauche-DCE. We may use a simple molecular geometry model for this estimation, which assumes that at a given field strength the molecular dipoles are reoriented toward the field direction by the same amount of tilt angle ($\Delta\theta$) for all gauche-DCE molecules. Molecules whose initial dipole direction ($\theta_0$) is close to the field direction ($\theta_0$

$\leq \Delta\theta$) are exempted from this assumption; they can be tilted only up to the field direction ($\theta_0 = \Delta\theta$). The procedure for calculating the RAIRS absorbance change with molecular tilt angle has been described previously.[16] The theoretical value of the relative absorbance change ($\Delta A/A_0$) as a function of the tilt angle is plotted in Figure 3-4. By comparing the theoretical $\Delta A/A_0$ curves with the experimental observation of $G_{\parallel}$ and $G_{\perp}$ band intensities, the average tilt angle for gauche-DCE molecules can be deduced.

The experimental $\Delta A/A_0$ value is calculated by dividing the field-induced absorbance change of $G_{\parallel}$ or $G_{\perp}$ band, shown by the blue curve in Figure 3-3, with the absorbance of corresponding bands for isotropic molecules ($A_0$). $A_0$ is the spectral absorbance of $G_{\parallel}$ (or $G_{\perp}$) band at zero field (Figure 3-1a) plus the absorbance contributed by the field-induced trans-to-gauche conversion (red curve in Figure 3-3). Here, we assume that the field-induced trans-to-gauche conversion generates isotropic gauche molecules. This assumption, however, may not be accurate because the trans-to-gauche conversion efficiency may be influenced by the molecular orientation and vice versa. For simplicity, the possibly entangled connection between trans-to-gauche conversion and molecular orientation is neglected. With this model, $\Delta A/A_0 \approx 36\%$ is calculated for the change of $G_{\parallel}$ band and $\Delta A/A_0 \approx -21\%$ for the change of $G_{\perp}$ band. These values correspond to an average tilt angle of 35° and 38°, respectively, according to the curves shown in Figure 3-4. The closeness of the two estimates for molecular tilt angle supports that the present model analysis is reasonable. We have imagined other possible mechanisms

that molecular reorientation may occur, for instance, the orientated gauche molecules are produced exclusively via trans-to-gauche conversion, whereas original gauche molecules in the sample are not reoriented by the field. In this case, very different tilt angles of 59 and 81° are expected from the observed changes in $G_{\parallel}$ and $G_{\perp}$ band intensities, respectively. For this reason, this possibility may be refuted.

The effect of temperature on the observed field-induced changes was examined. Figure 3-5 compares the field difference spectra of DCE samples that were prepared and analyzed at three temperatures: 8, 50, and 90 K. The field-induced spectral changes were negligible at 8 K, indicating that molecular conformation and orientation did not change. The field-induced changes started to appear to an appreciable extent above 50 K and further intensified at 90 K. The experiment was not conducted above 90 K because the dielectric relaxation of $D_2O$ layers in the samples occurring above 90 K drastically reduced the field strength across the DCE film.[20]

We observed that the field-induced conformational and orientational changes were irreversible with respect to the changes of temperature and field. When the field-induced changes were observed at high temperature and then the sample temperature was reduced, the spectral changes were not reversed. Also, a decrease of applied field strength did not return to the original spectrum at the weaker field. A similar irreversible behavior has been reported for field-induced reorientation of acetone in frozen molecular solid.[16]

The temperature dependence shown in Figure 3-5 indicates that both electric field and thermal energy are needed to facilitate the molecular orientation and conformation changes. Also, it shows that DCE molecules in the sample are not in dipolar equilibrium with the applied field at the present temperatures. The dipole flipping energy of gauche-DCE is 0.6 kJ $mol^{-1}$ at the field strength of $1.5 \times 10^8$ V $m^{-1}$. This energy is comparable with thermal energy (< 0.7 kJ $mol^{-1}$ at < 90 K), but lower than the kinetic barrier of C-C bond rotation for the trans-to-gauche conversion in liquids (~10 kJ $mol^{-1}$).[10] Therefore, we interpret that the nonoccurrence of orientational and conformational changes observed at low temperature is mainly due to a kinetic barrier, rather than a thermodynamic energy difference, of the transformation. Extra thermal energy is needed to activate molecular motion and to overcome the kinetic barrier.[24] The observed irreversibility with respect to the temperature and field changes also supports the presence of a kinetic barrier.

The kinetic barrier is associated with intermolecular interactions in the condensed phase. The intermolecular interactions generate quite strong, directional electric fields to molecules, for example, in the range of $5–30 \times 10^8$ V $m^{-1}$ for polar solvent molecules, as estimated from the Stark effect and solvatochromism of the vibrational bands of chromophore molecules.[23] Such a strong internal field can effectively resist the change imposed by external field. The internal field can also act as a driving force for spontaneous changes that occur during the sample heating. Molecules in condensed molecular films are shallowly trapped in the local energy minima of potential energy surface. Given the mobility at high temperature, these molecules in metastable

structures are relaxed to more stable structures guided by intermolecular forces. The change in spectral absorbance induced by external field (Figure 3-1) was comparable in magnitude to that induced by sample heating (Figure 3-2). This means that the external field changed the molecular conformation and orientation to a comparable degree to the effect of internal field on the changes during heating.

## III-4. Summary

(i) The ice film capacitor method was used in combination with RAIRS measurement to investigate the conformational and orientational changes of DCE induced by electric field in frozen molecular solid. The electric field changed trans-DCE molecules to gauche conformers by inducing C-C bond rotation via electrostatic interaction. The conversion efficiency of this process was 24% at $1.5 \times 10^8$ V $m^{-1}$ at 75 K.

(ii) The applied field also changed the dipole orientation of gauche-DCE molecules toward the field direction. Each degree of molecular reorientation and trans-to-gauche conversion was quantified by deconvoluting the field difference spectrum against the thermal difference spectrum that measured the trans-to-gauche conversion at zero field. A simple molecular geometry model estimated the average tilt angle of gauche-DCE molecules to be 35-38°.

(iii) The observed conformational and orientational changes are very large compared to those achieved for liquid samples at weaker fields in previous studies.[11-12] The changes induced by external field at ~$10^8$ V $m^{-1}$ are

comparable in magnitude to those driven by intermolecular interactions in molecular solid during thermal heating of the sample. The present study suggests the possibility of brute force manipulation of molecular conformation and orientation in a frozen molecular solid using the external field.

## Reference


1. Dugave, C.; Demange, L., *Chem. Rev.* **2003**, *103*, 2475.
2. Fischer, G., *Chem. Soc. Rev.* **2000**, *29*, 119.
3. Hasha, D.; Eguchi, T.; Jonas, J., *J. Am. Chem. Soc.* **1982**, *104*.
4. Todd, D. C.; Fleming, G. R., *J. Chem. Phys.* **1993**, *98*, 269.
5. Depaepe, J.-M.; Ryckaert, J.-P., *Chem. Phys. Lett.* **1995**, *245*, 653.
6. Long, S. B.; Campbell, E. B.; MacKinnon, R., *Science* **2005**, *309*, 903.
7. Cha, A.; Snyder, G. E.; Selvin, P. R.; Bezanilla, F., *Nature* **1999**, *402*, 809.
8. Bard, A. J.; Puglisi, V. J.; Kenkel, J. V.; Lomax, A., *Faraday Discussions of the Chemical Society* **1973**, *56*, 353.
9. Tong, X.; Pelletier, M.; Lasia, A.; Zhao, Y., *Angew. Chem. Int. Ed.* **2008**, *47*, 3596.
10. Alemani, M.; Peters, M. V.; Hecht, S.; Rieder, K.-H.; Moresco, F.; Grill, L., *JACS* **2006**, *128*, 14446.
11. Hiramatsu, H.; Kato, C.; Hamaguchi, H., *Chem. Phys. Lett.* **2001**, *347*, 403.
12. Hiramatsu, H.; Hamaguchi, H.-o., *Appl. Spectrosc.* **2004**, *58*, 355.
13. Lee, I.-C.; Hamaguchi, H.-o.; Shigeto, S., *Chem. Phys. Lett.* **2008**, *466*, 144.
14. Lee, J. Y.; Yoshida, N.; Hirata, F., *J. Phys. Chem. B* **2006**, *110*, 16018.
15. Shin, S.; Kim, Y.; Moon, E.-s.; Lee, D. H.; Kang, H.; Kang, H., *J. Chem. Phys.* **2013**, *139*, 074201.
16. Shin, S.; Kim, Y.; Kang, H.; Kang, H., *J. Phys. Chem. C* **2015**, *119*,

15588.

17. Shin, S.; Kang, H.; Cho, D.; Lee, J. Y.; Kang, H., *J. Phys. Chem. C* **2015**, *119*, 15596.

18. Kang, H.; Shin, S.; Park, Y.; Kang, H., *J. Phys. Chem. C* **2016**, *120*, 17579.

19. Zimbitas, G.; Haq, S.; Hodgson, A., *J. Chem. Phys.* **2005**, *123*.

20. Tsekouras, A. A.; Iedema, M. J.; Cowin, J. P., *Phys. Rev. Lett.* **1998**, *80*, 5798.

21. Shimanouchi, T., *Tables of Molecular Vibrational Frequencies*. National Bureau of Standards: **1972**.

22. Park, S. C.; Moon, E. S.; Kang, H., *Phys. Chem. Chem. Phys.* **2010**, *12*, 12000.

23. Fried, S. D.; Bagchi, S.; Boxer, S. G., *JACS* **2013**, *135*, 11181.

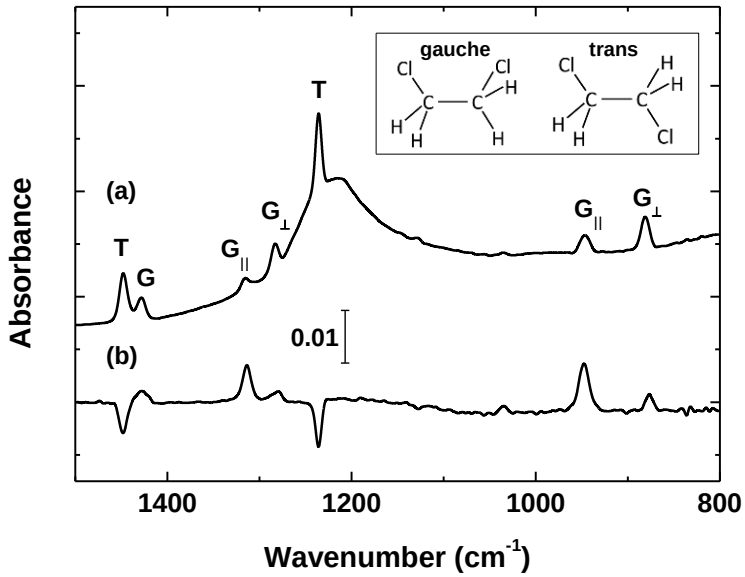


**Figure 3-1**. (a) RAIR spectrum of a DCE film (29 ML thickness) that was sandwiched between $D_2O$ films (38 ML thickness). (b) The field difference spectrum, which is the absorbance difference between the field-on and field-off spectrum. The difference spectrum is shown at 3× magnification. The applied electric field across the DCE film was $1.5 \times 10^8$ . The temperature of sample preparation and spectral acquisition was 75 K. The inset shows the molecular structures of gauche- and trans-DCE.

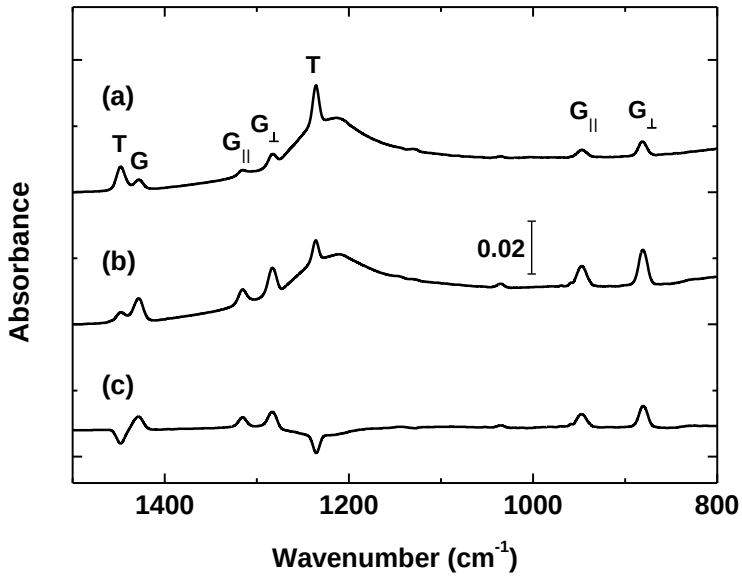


**Figure 3-2**. (a) RAIR spectrum of a DCE film (30 ML) prepared at 55 K. (b) RAIR spectrum after heating the sample at 90 K. (c) A thermal difference spectrum obtained by subtracting spectrum (a) from (b).

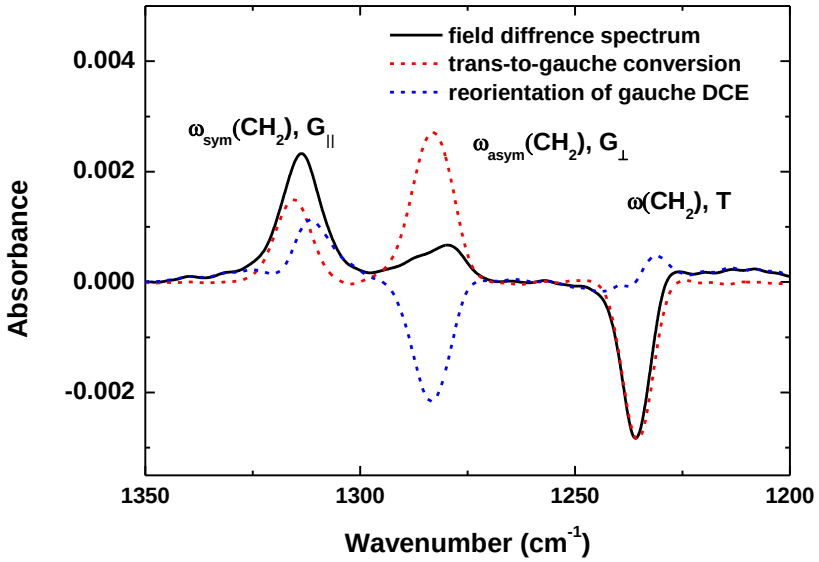


**Figure 3-3**. Spectral analysis of the $CH_2$ wagging bands of DCE in the field difference spectrum (black line). The contributions of the trans-to-gauche conversion (red dashed line) and the reorientation of gauche conformer (blue dashed line) are shown.

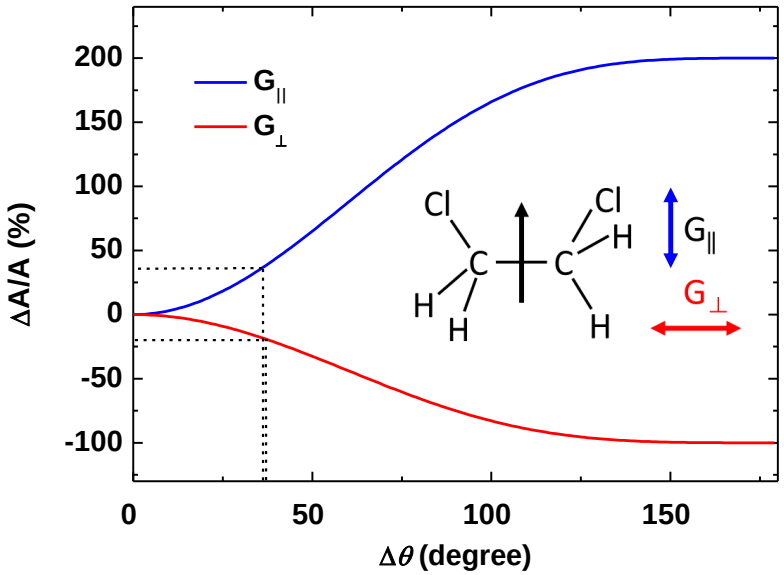


**Figure 3-4**. Theoretical curve of relative absorbance change ($\Delta A/A_0$) versus average tilt angle ($\Delta\theta$) of permanent dipole of gauche-DCE. The curve for $G_{\parallel}$ band is shown in blue, and $G_{\perp}$ band, in red. The molecular dipole direction is indicated by a black arrow. The directions of transition dipole moments of $G_{\parallel}$ and $G_{\perp}$ vibrations are indicated by blue and red double-ended arrows, respectively. The experimental $\Delta A/A_0$ values are marked with dotted lines.

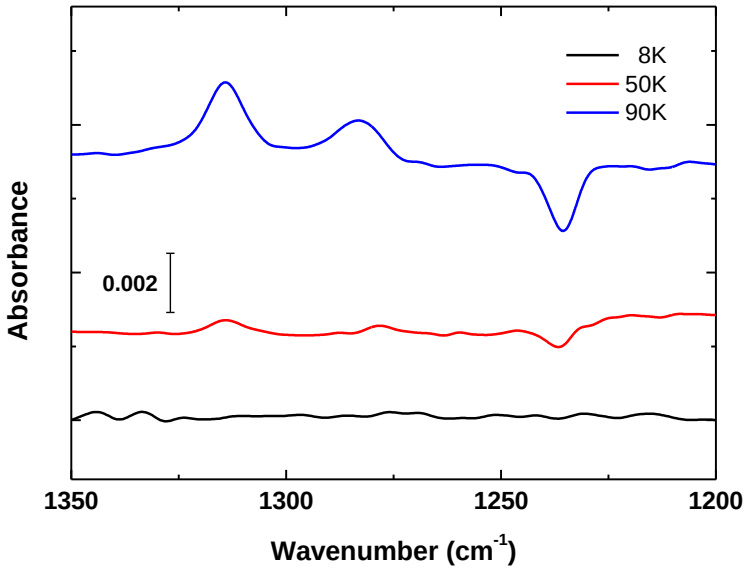


**Figure 3-5**. The field difference spectra for the $CH_2$ wagging bands of DCE samples at three temperatures (8, 50, and 90 K). The sample preparation and spectral acquisition were made at the same indicated temperature. The applied field strength was approximately $1 \times 10^8$ V $m^{-1}$.

# Chapter IV

# Field-Induced Acid Dissociation at the Acid-Base Interface

## Abstract

We studied the effect of applied electric field on the dissociation of acetic acid (AA) using the ice film capacitor method. The dissociation of AA was monitored using reflection absorption infrared spectroscopy (RAIRS), which measured changes in the intensities of the vibrational modes of AA and acetate anion ($AA^-$). The amount of field-induced dissociation depended on the direction of the applied electric field. Interestingly, the acid dissociation yield was greater when the field was applied in the opposite direction to the proton transfer motion. This suggests that the reaction was aided by the reorientation of reagent molecules rather than by electrostatic stabilization of the charge transfer energy. The effect of molecular size was studied by comparing the results for formic acid and propionic acid with those obtained for AA. The dissociation of smaller acids was more strongly enhanced than that of larger

acids, supporting the interpretation that field-induced dissociation occurred via molecular reorientation.

## IV-1. Introduction

The effect of externally applied electric fields on chemical reactions has been studied for a long time. For example, in the 1930s, Wien[1] observed that dissociation constants of weak electrolytes increased under strong electric fields. This phenomenon, known as the second Wien effect, was explained by Onsager[2] using a theoretical model that suggests the field decreases the probability of the recombination of dissociated ions via diffusion. Simons[3] studied the proton transfer between water and ion-exchange membranes and observed a significant enhancement of ionic current in the presence of an external electric field. It was claimed that proton transfer was accelerated by the second Wien effect and/or the alignment of water molecules along the electric field at the membranes. This work, however, has not been followed up with further rigorous investigations in the physical chemistry research community. Recently, Stuve[4] studied the emission of field-ionized hydrated proton clusters $[H^+(H_2O)_n]$ from a Pt tip coated with water layer. The observations suggested an increased degree of autoprotolysis of water under the extraordinarily strong fields ($\sim 10^{10}\ V \cdot m^{-1}$) present at the tip apex. Boxer and coworkers[5] studied the vibrational Stark effect of molecules in frozen films under strong electric fields ($\leq 1 \times 10^8\ V \cdot m^{-1}$). They proposed that electric fields at the active sites of enzymes play a crucial role in a ketosteroid isomerase reaction by stabilizing a transition state complex.

Despite extensive studies on field effects, the mechanisms by which electric fields operate on reactions are not clearly revealed in many cases. In the case of acid-base reactions, an interesting question is how the electric field,

internal or external, affects proton transfer from the acid to the base. Does the field lower the electrostatic energy of proton displacement, or does it affect the reaction path by other means? In this paper, we study the effect of external electric fields on acid-base reactions by preparing molecular films of carboxylic acids and ammonia and applying strong electric fields (~$10^8$ $V \cdot m^{-1}$) across the samples using the ice film capacitor method. Reflection absorption infrared spectroscopy (RAIRS) is used to monitor the field effect by measuring the progress of the reactions.

## IV-2. Experimental Methods

All experiments were conducted in an ultra-high vacuum (UHV) chamber with a background pressure of below $1 \times 10^{-10}$ Torr, which was equipped with instrumentations for reflection absorption infrared spectroscopy (RAIRS), Kelvin work function measurements, temperature-programmed desorption (TPD) mass spectrometry.[6] A molecular film sample was deposited on a Pt(111) single crystal surface maintained at 70 K inside the UHV chamber. The Pt(111) surface was cleaned using sputtering and annealing procedures, and its cleanliness was verified from the TPD profile of the $D_2O$ monolayer formed on the surface.[7]

Acetic acid ($CH_3COOH$; AA), formic acid (HCOOH; FA), propionic acid ($CH_3CH_2COOH$; PA), and $NH_3$ vapors were introduced close to the Pt(111) substrate surface by using a tube doser and were deposited at rates below 0.1 $ML \cdot s^{-1}$ (monolayer per second). The $D_2O$ film was deposited using

a backfilling method at a deposition rate below 0.2 ML·s$^{-1}$. The thicknesses of the molecular films were estimated from the TPD measurements. The thickness of the $D_2O$ film was determined by comparing its TPD intensity with that of a $D_2O$ monolayer on Pt(111).[7] For the acid and $NH_3$ films, mole-to-thickness conversions were made using the unit cell volumes of their crystals.[8-11] The film thicknesses are expressed in units of ML in this paper, where 1 ML represents $1.1 \times 10^{15}$ molecules cm$^{-2}$ for $D_2O$, $4.7 \times 10^{14}$ molecules cm$^{-2}$ for FA, $3.5 \times 10^{14}$ molecules cm$^{-2}$ for AA, $3.1 \times 10^{14}$ molecules cm$^{-2}$ for PA, and $7.8 \times 10^{14}$ molecules cm$^{-2}$ for $NH_3$.

Electric fields were applied across the frozen molecular films using the ice film capacitor method, which was described in detail in a previous paper.[6, 12] The field strength was increased by the deposition of $Cs^+$ ions on the $D_2O$ film surface using a low energy $Cs^+$ ion gun. The field strength was decreased by exposing the $Cs^+$-deposited film to 5 eV electrons. We prepared a sample composed of multiple stacks of acid and $NH_3$ films to study the electric field-induced dissociation of acids at the interface between an acid film and an $NH_3$ film. The layered film was sandwiched between two amorphous solid $D_2O$ films to prevent direct contact with the Pt substrate or cesium ions. To prepare the sample, a 41 ML $D_2O$ amorphous solid water (ASW) film was grown on a Pt(111) substrate at 70 K, following which a 12 ML-thick $NH_3$ film was grown over the ASW film at the same temperature. Then, a 20 ML-thick acid film was overlaid on the $NH_3$ film, and finally a 41 ML $D_2O$ film was used to cover the acid film. In this paper, we denote this $D_2O$/acid/$NH_3$/$D_2O$/Pt(111) layered film as an "acid(top)/$NH_3$(bottom)

layered film." For samples composed of different dielectric layers, the electric field strength inside a certain layer (*e.g.*, the acid layer) can be expressed as:

$$F_{acid} = \Delta\text{CPD}/[d_{acid} + d_{NH_3}\frac{\varepsilon_{acid}}{\varepsilon_{NH_3}} + d_{D_2O}\frac{\varepsilon_{acid}}{\varepsilon_{D_2O}}]$$

In the above equation, ΔCPD is the voltage across the whole film, $d_{acid}$, $d_{NH_3}$, and $d_{D_2O}$ are the thicknesses of acid, $NH_3$, and $D_2O$ films, respectively, and $\varepsilon_{acid}$, $\varepsilon_{NH_3}$, and $\varepsilon_{D_2O}$ are their dielectric constants. Since the dielectric constants for frozen acids and $NH_3$ films have not been reported, we estimated their dielectric constants using the Clausius-Mossotti relation:

$$\frac{\varepsilon_r - 1}{\varepsilon_r + 2} = \frac{N\alpha}{3\varepsilon_0}$$

where $\alpha$ is the polarizability,[13] and $N$ is the number density of the molecule. The dielectric constant for solid $D_2O$ was also estimated in the same manner. The electric field at the interface between two films was determined from the average value of the electric fields in the two films.

RAIRS measurements were performed in a grazing angle (84°) reflection geometry using a commercial Fourier-transform infrared (FTIR) spectrometer with a mercury-cadmium telluride detector. The incident IR beam was linearly p-polarized using a wire grid polarizer. The beam path outside the UHV chamber was purged with dry $N_2$ gas to remove other IR active gases. RAIR spectra were averaged 256 times at a spectral resolution of 4 $cm^{-1}$.

## IV-3. Results

We prepared various samples containing molecular and ionized forms of AA and recorded their RAIR spectra in order to use them as spectral references for monitoring the acid-base reaction. AA molecules dissociate into acetate ($AA^-$) and ammonium ($NH_4^+$) ions when in contact with $NH_3$ molecules. This ionic dissociation of AA was studied by monitoring the changes seen in the vibrational modes of AA and $AA^-$. Figure 4-1 shows the vibrational modes in AA and $AA^-$. The peak positions of each vibrational mode were consistent with those reported in previous studies.[14-15] A pure AA film showed a carboxyl double bond stretching mode (1727 $cm^{-1}$, ν(C=O)), as shown in Figure 4-1(a), and a hydroxyl stretching mode (3100–3200 $cm^{-1}$, ν(OH)) (outside the range displayed). The existence of ν(C=O) and ν(OH) modes indicates that AA molecules existed in their molecular form in the pure AA film. In the case of a 1:20 AA-$NH_3$ mixture, shown in Figure 4-1(b), these ν(C=O) and ν(OH) modes disappeared and a new peak was observed at 1565 $cm^{-1}$, which was assigned to antisymmetric CO stretching (ν(CO)) in $AA^-$.[15] The peak at 1652 $cm^{-1}$ was assigned to an NHN scissoring mode ($\nu_2$) of $NH_3$. These vibrational features indicate that AA molecules dissociated in an $NH_3$ solvation environment and existed as $AA^-$ ions.

The IR spectrum of an "AA(top)/$NH_3$(bottom)" layered film is shown in Figure 4-1(c). This sample showed strong absorbance for the ν(C=O) band of AA and weak absorbance for the ν(CO) mode of $AA^-$. The weak ν(CO) intensity of the $AA^-$ indicates that AA molecules at the AA-$NH_3$ interface

produced acetate ions. The dissociation of AA at the $D_2O$-AA interface did not occur, which was verified by the lack of an ν(CO) peak of $AA^-$ in a $D_2O$/AA/$D_2O$ sandwiched film (see Supporting Information Figure 4-S1).

We estimated the thickness of the reactive boundary region of the $NH_3$-AA interface, in which acid-base reaction between AA and $NH_3$ spontaneously occurs. Changes in the intensity of the ν(C=O) peak in AA and the ν(CO) peak in $AA^-$ were measured according to the thickness of the AA film on the $NH_3$ film. AA molecules were deposited on $NH_3$ samples at 70 K. Figure 4-2(a) shows the changes in the absorbance when the AA film thickness was changed from x ML to y ML.

When we deposited a 1.3 ML AA film on the $NH_3$ film, the intensity of the ν(CO) in $AA^-$ peak increased while the ν(C=O) in AA peak did not noticeably increase, indicating that most of the AA molecules present on the $NH_3$ surface were dissociated. As the AA film thickness was increased, the intensity of the ν(C=O) in AA peak began to increase, showing that some of the AA molecules did not dissociate on the film. These AA molecules could either have been located within the molecular AA film or existed on the $NH_3$ surface with molecular geometries that were unfavorable for proton transfer to $NH_3$. The intensity of the ν(CO) in $AA^-$ peak did not increase above AA film thicknesses of 5 ML, meaning that the $NH_3$ surface was fully covered with AA molecules and that only molecular AA films were made at greater film thicknesses. These observations verified that AA molecules did not mix with $NH_3$ during sample preparation and that the $NH_3$-AA interface consisted of sequential depositions as intended. From the saturated absorbance area of the

ν(CO) in $AA^-$ peak, the density of $AA^-$ molecules at the interface was estimated to be $1.4 \times 10^{15}$ molecules $cm^{-2}$, four times larger than seen in an AA monolayer.[9] The presence of wrinkles at the interface may have increased the effective interfacial area. With this effect included, we may consider that the thickness of reactive boundary phase of the interface was approximately 4 ML.

The effect of the electric field on acid dissociation was examined using AA-$NH_3$ layered films. External electric fields were applied to the layered film using the ice film capacitor method.[6] In our experimental setup, the direction of the applied electric field was fixed from the sample/vacuum interface, where $Cs^+$ ions were deposited, to the sample/metal interface, where negative counter charges were drawn. To change the direction of the applied field, the stacking sequence of the AA and $NH_3$ films in the sample was reversed. We indicate the field direction by marking the bias polarity of the samples, for instance, "(+)$NH_3$/AA(–)" represents a charged $NH_3$(top)/AA(bottom) film, while "(+)AA/$NH_3$(–)" represents a charged AA(top)/$NH_3$(bottom) film.

Figure 4-3(a) shows the RAIR spectrum of an $NH_3$(top, 12 ML)/AA(bottom, 25 ML) layered film and a difference spectrum at $F = 1.2 \times 10^8$ $Vm^{-1}$. The difference spectrum, which shows the absorbance difference between the field-on and field-off spectra, indicates that the absorbance of the CO stretching mode in $AA^-$ increased and the absorbance of the ν(C=O) mode in AA decreased when applying an electric field. These changes indicate that neutral AA molecules at the reactive boundary region were dissociated into acetate ions by the external electric field. This dissociation was irreversible

when the field strength was decreased from $1.2 \times 10^8$ $Vm^{-1}$ to $4 \times 10^7$ $Vm^{-1}$ (not shown). The relative absorbance changes at different field strengths are shown in Figure 4-3(b) in the case of (+)$NH_3$/AA(–) and (+)AA/$NH_3$(–). The amount of field-induced AA dissociation was quantified based on the change in the absorbance of the ν(CO) in $AA^-$ peak. The entire RAIR spectra and their difference spectra are reported in the Supporting Information (Figure 4-S3). Both the $NH_3$(top)/AA(bottom) and the AA(top)/$NH_3$(bottom) layered films showed increases in the intensity of the ν(CO) in $AA^-$ with increasing field strength.

However, the extent of AA dissociation was different depending on the field direction. For example, at a field strength of $1.2 \times 10^8$ $Vm^{-1}$, the relative absorbance of the ν(CO) peak increased by 38% for (+)$NH_3$/AA(–) and 13% for (+)AA/$NH_3$(–). The RAIR spectrum of the $NH_3$(top)/AA(bottom) sample shown in Figure 4-3(a) is almost identical to that of the AA(top)/$NH_3$(bottom) sample in Figure 4-1(c), and the absorption areas of the ν(CO) peaks of $AA^-$ in the two films were within 10% of each other. These observations verified that the structures of the reactive boundary regions in both films were identical. Therefore, the difference between the amounts of AA dissociation was caused by the direction of the electric field.

The vibrational Stark effect (VSE) was also observed for the vibrational bands of AA and $NH_3$ under the external electric field (Supporting Information Figures 4-S1 and 4-S2). The VSE appears as band broadening due to the ensemble average of Stark frequency shifts of randomly oriented molecules.[16-18] The VSE was reversible when the field was increased and

decreased, as would be expected.

Field-induced dissociation was also studied for formic acid (FA) and propionic acid (PA). Figure 4-4(a) shows the RAIR spectra of $NH_3$(top)/FA(bottom) and $NH_3$(top)/PA(bottom) layered films and their difference spectra at an electric field strength of $1.4 \times 10^8$ $Vm^{-1}$. The positions of the ν(C=O) peaks in FA and PA were 1737 $cm^{-1}$ and 1721 $cm^{-1}$, respectively. These carboxylic acids also dissociated at the acid-$NH_3$ interface, and existed as formate ($FA^-$) or propionate ($PA^-$). The ν(CO) peak positions in $FA^-$ and $PA^-$ were 1595 $cm^{-1}$ and 1560 $cm^{-1}$, respectively.

When we applied electric fields to these films, field-induced dissociation occurred in a similar way to that which was seen for the AA-$NH_3$ layered film. Figure 4-4(b) shows the relative absorbance changes in various carboxylic acid-$NH_3$ layered films at different field strengths. For all carboxylic acids, field-induced dissociation was enhanced by increasing the applied electric field strength. Formic acid molecules showed the largest enhancement (62% at $1.4 \times 10^8$ $Vm^{-1}$), and propionic acid molecules showed the lowest enhancement (36% at $1.4 \times 10^8$ $Vm^{-1}$). All RAIR spectra and their difference spectra are reported in Figure 4-S4.

## IV-4. Discussion

The experimental measurements in the present study show that external electric field can increase the dissociation of acids in acid-base interfacial

regions. One plausible explanation for this phenomenon is that the applied field electrostatically influences proton transfer across the H-bond of an acid-base pair.[19-20] Figure 4-5(a) illustrates this "electrostatic mechanism." When the H-bond of an AA-$NH_3$ pair is properly aligned along the field, the electrostatic interaction between the partially charged transition state (TS) and the external field will lower the energy barrier of proton transfer and stabilize the product. This direct field-induced mechanism was proposed for the occurrence of molecular isomerization in the active sites of proteins (the "field catalysis mechanism")[5] and the field-induced ionization at a scanning tunneling microscope tip.[21] However, this mechanism is not consistent with our experimental results. According to this mechanism, AA molecules in the (+)AA/$NH_3$(–) sample would dissociate more easily than those in the (+)$NH_3$/AA(–) sample due to the favorable direction of the applied electric field. In contrast, AA molecules in the (+)$NH_3$/AA(–) sample dissociated more efficiently (Figure 4-3(b)), meaning that field-induced dissociation did not occur via the electrostatic mechanism.

An alternative possibility is that the acid dissociation occurred via reorientation of molecules under the applied field. Figure 4-5(b) illustrates this "reorientation mechanism." For acid dissociation to occur, adjacent AA and $NH_3$ molecules should have suitable orientations–such that the OH group of AA points toward the lone electron pair of $NH_3$. However, a substantial portion of AA-$NH_3$ pairs in the reactive boundary region will not have these favorable orientations because the sample was prepared by random deposition of gas molecules on a cold substrate surface. Therefore, the activation barrier for

proton transfer will be very large for typical AA-$NH_3$ pairs in this situation. By applying an external electric field, a certain portion of AA molecules can be reoriented along the field, bringing the OH group close to the lone pair of $NH_3$. In this favorable configuration, proton transfer from AA to $NH_3$ is energetically favorable and thus occurs spontaneously and irreversibly. This mechanism is consistent with our experimental results regarding the direction of the field.

In support of the reorientation mechanism, it has been shown that the reorientation of small polar molecules in frozen molecular films can occur under external electric fields of $10^8$ $Vm^{-1}$.[12] The significant dependence of the field-induced acid dissociation on molecular size, shown in Figure 4-4(b), is also consistent with the reorientation mechanism. Molecular reorientation is severely hindered in frozen molecular films due to interactions with neighboring molecules. The observed field-induced effect had the order FA > AA > PA (Figure 4-4(b)), *i.e.*, smaller acids exhibited a stronger effect because they were more easily reoriented by the field. Consider the decrease in energy by the electrostatic mechanism. The applied field can change the electrostatic energy for the ionic dissociation of a bond by ~1 kJ/mol at $10^8$ $Vm^{-1}$. This change is very small compared to the overall reaction energy of acid dissociation, and thus this decrease will not significantly affect the reaction. It is considered that an electric field strength of $10^9$–$10^{10}$ $Vm^{-1}$ would be needed for the electrostatic mechanism to be observed.[4-5]

A small increase in acid dissociation was observed even when field-induced molecular reorientation might be expected to produce the opposite

effect, for example in the (+)AA/$NH_3$(–) sample. The fact that the AA/$NH_3$ interface was wrinkled rather than flat may explain this deviation from ideal behavior. As shown in Figure 4-2, the effective areas of the interfaces were large, meaning that AA-$NH_3$ pairs were not perfectly aligned as would be expected for an ideal interface. In this case, a small portion of the pairs may sit in reversed positions, and their reactions could be triggered by the opposite field. In addition, the reorientation of $NH_3$ molecules may occur, leading to field-induced acid dissociation.

It is worth considering why field-induced acid dissociation occurs via an indirect molecular reorientation mechanism rather than a direct electrostatic mechanism from the viewpoint of reaction dynamics. When an acid-base reaction occurs thermally in a molecular solid, proton transfer from the acid to the base occurs instantaneously compared to the thermal reorientation of molecules, which is very slow. Therefore, if an external field is applied to the system, the perturbation effect will naturally appear most pronouncedly for the rate-determining step, which is the molecular reorientation, with the effect on the proton transfer step being almost invisible in the overall reaction rate. There is some degree of analogy between the proton transfer reaction in the solid phase and the electron transfer reaction in the liquid phase, where electron transfer occurs on a much faster time scale than solvent reorganization. In this case, solvent motion becomes the rate-determining reaction coordinate, and the solvent reorganization energy becomes the overall activation energy. The indirect field-induced mechanism in the present study is also reminiscent of the molecular mechanism of the second Wien effect of electrolyte

dissociation in solution, as explained by Onsagar.[2] There, the external electric field increases the extent of electrolyte dissociation by primarily affecting the diffusion kinetics of ions rather than the bond breaking process itself. The field reduces the probability of recombination of slowly diffusing ions and, as such, favors irreversible formation of solvent-separated ion pairs. A general lesson that could be learned from these parallel examples is that for reactions in condensed-phases, the applied electric field mostly affects the kinetics, rather than the energetics, of a reaction.

## IV-5. Conclusion

The effect of applied electric field on the dissociation of carboxylic acids was studied by monitoring the vibrational bands of acids located at the interface of frozen molecular films of acid and base. The degree of acid dissociation increased with increasing applied field strength. In addition, the degree of acid dissociation enhancement depended on the direction of the field. Interestingly, the enhancement effect was greater when the field was applied in the opposite direction to the proton transfer motion. The enhancement effect was examined for carboxylic acids with different molecular sizes, with stronger effects being observed for smaller acids. The observations indicate that field-induced acid dissociation does not occur because of the energy barrier of proton transfer being lowered via electrostatic interactions between the acid-base pair and the applied field. Rather, the field changes the orientation of the acid and base molecules at the interface, triggering spontaneous proton transfer.

## Reference


1. Wien, M., *Phys. Zeits* **1928**, *29*, 751.
2. Onsager, L., *J. Chem. Phys.* **1934**, *2*, 599.
3. Simons, R., *Nature* **1979**, *280*, 824.
4. Stuve, E. M., *Chem. Phys. Lett.* **2012**, *519*, 1.
5. Fried, S. D.; Bagchi, S.; Boxer, S. G., *Science* **2014**, *346*, 1510.
6. Shin, S.; Kim, Y.; Moon, E.-s.; Lee, D. H.; Kang, H.; Kang, H., *J. Chem. Phys.* **2013**, *139*, 074201.
7. Haq, S.; Harnett, J.; Hodgson, A., *Surf. Sci.* **2002**, *505*, 171.
8. Holtzberg, F. v.; Post, B.; Fankuchen, I., *Acta Crystallographica* **1953**, *6*, 127.
9. Jones, R. E.; Templeton, D. H., *Acta Crystallographica* **1958**, *11*, 484.
10. Strieter, F. J.; Templeton, D. H.; Scheuerman, R.; Sass, R, *Acta Crystallographica* **1962**, *15*, 1233.
11. Hewat, A.; Riekel, C., *Acta Crystallographica Section A* **1979**, *35*, 569.
12. Shin, S.; Kim, Y.; Kang, H.; Kang, H, *J. Phys. Chem. C* **2015**, *119*, 15588.
13. Gussoni, M.; Rui, M.; Zerbi, G., *J. Mol. Struct.* **1998**, *447*, 163.
14. Garcia, A.; Da Silva, J.; Ilharco, L., *Surf. Sci.* **1998**, *415*, 183.
15. Ito, K.; Bernstein, H. J., *Can. J. Chem.* **1956**, *34*, 170.
16. Boxer, S. G., *J. Phys. Chem. B* **2009**, *113*, 2972.
17. Shin, S.; Kang, H.; Cho, D.; Lee, J. Y.; Kang, H., *J. Phys. Chem. C* **2015**, *119*, 15596.
18. Andrews, S. S.; Boxer, S. G., *J. Phys. Chem. A* **2000**, *104*, 11853.
19. Fried, S. D.; Boxer, S. G., *Annu. Rev. Biochem* **2017**, *86*, 387.
20. Henstridge, M. C.; Laborda, E.; Rees, N. V.; Compton, R. G.,

*Electrochim. Acta* **2012**, *84*, 12.

21. Plummer, M.; McCann, J. F., *Journal of Physics B: Atomic, Molecular and Optical Physics* **1996**, *29*, 4625.

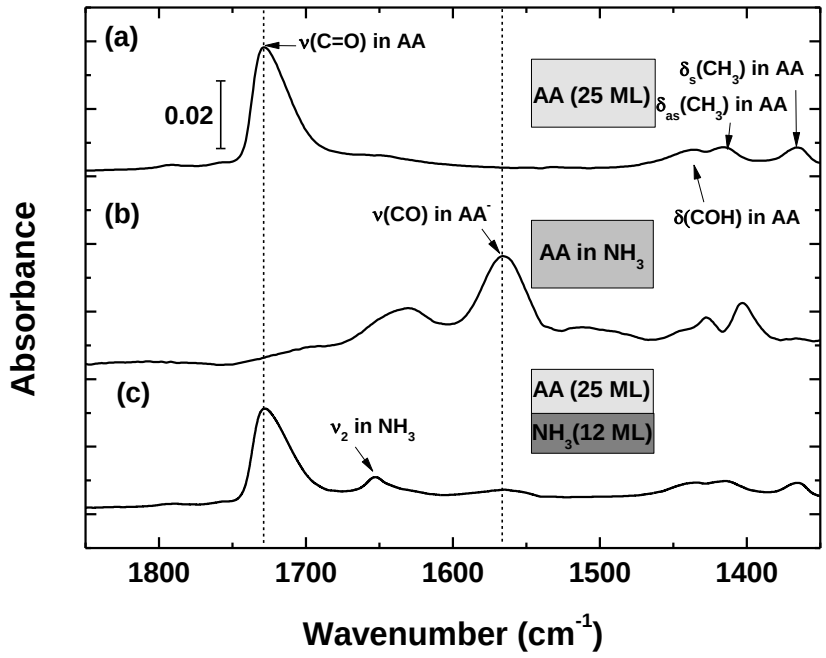


**Figure 4-1.** RAIR spectra of various AA samples between 1900 $cm^{-1}$ and 1350 $cm^{-1}$. Eachsample was prepared on a Pt (111) surface at 70 K. (a) A pure AA film (25 ML) (b) A mixed AA-$NH_3$ film with an AA:$NH_3$ molar ratio of 1:20. (c) An "AA(top)/$NH_3$(bottom)" sample, with a structure of $D_2O$ (41 ML)/AA (25 ML)/$NH_3$ (12 ML)/$D_2O$ (41ML)/Pt(111).

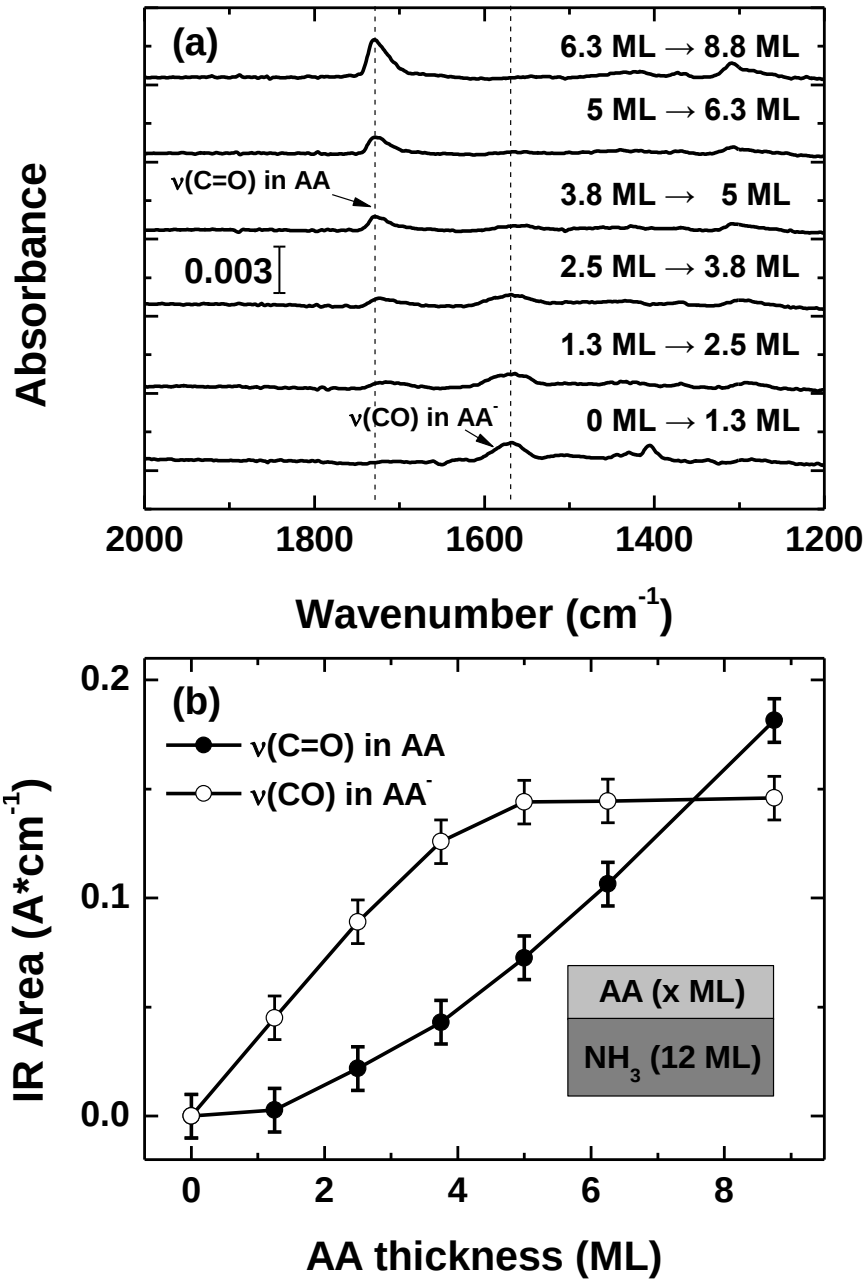


**Figure 4-2.** (a) Changes in RAIR spectra as the thickness of the AA film on the $NH_3$ film increased. Spectra marked "x ML → y ML" show the absorbance

change when the AA film thickness was changed from x ML to y ML. (b) Intensity changes of the ν(C=O) in AA and ν(CO) in $AA^-$ peaks according to AA film thickness.

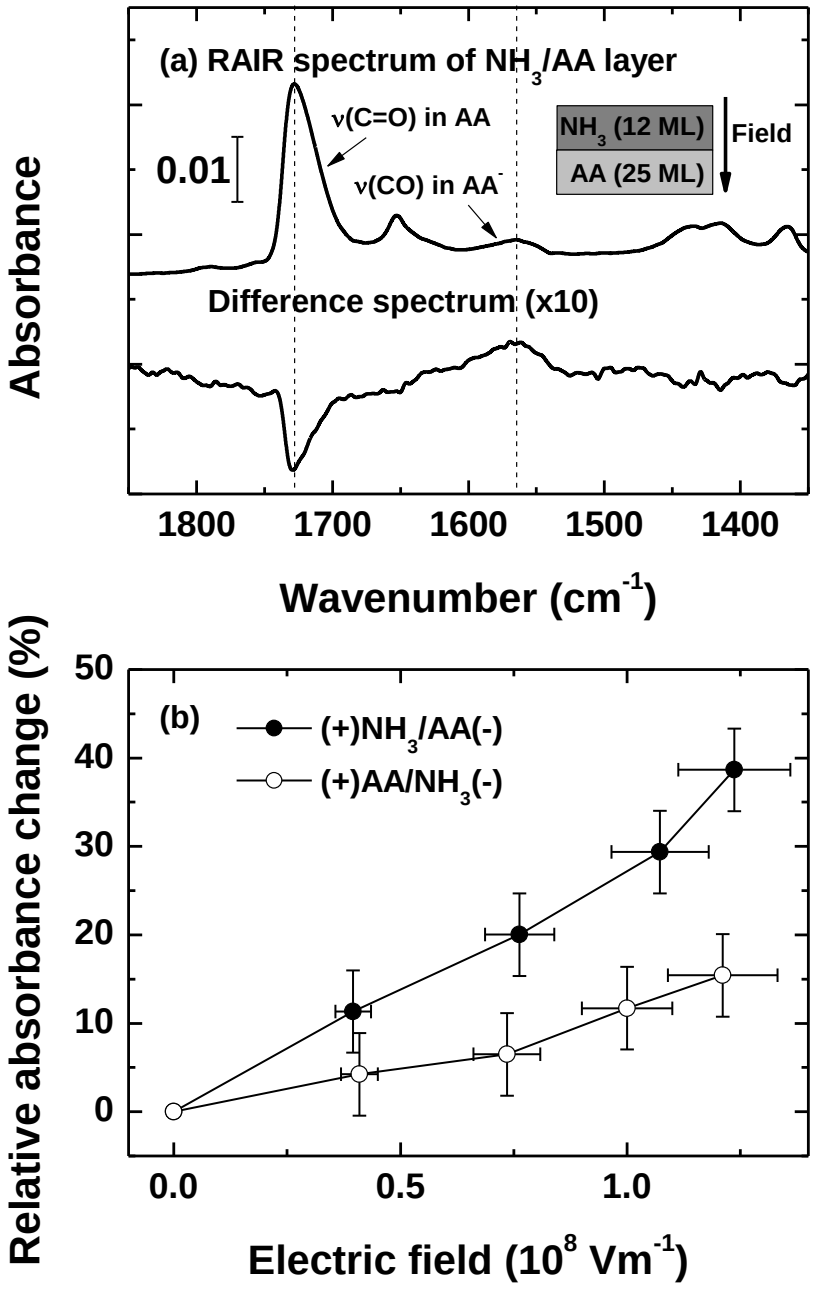


**Figure 4-3.** (a) (Top) RAIR spectrum of an $NH_3$(top, 12 ML)/AA(bottom, 25 ML) layered film. (Bottom) The field-on minus field-off difference spectrum.

The difference spectrum was magnified by a factor of ten. (b) Relative absorbance changes in the $\nu$(CO) in $AA^-$ as a function of the applied electric field strength. To change the direction of the applied field, the stacking sequence of the AA and $NH_3$ films was reversed. The field directions are indicated as (+)$NH_3$/AA(–) and (+)AA/$NH_3$(–).

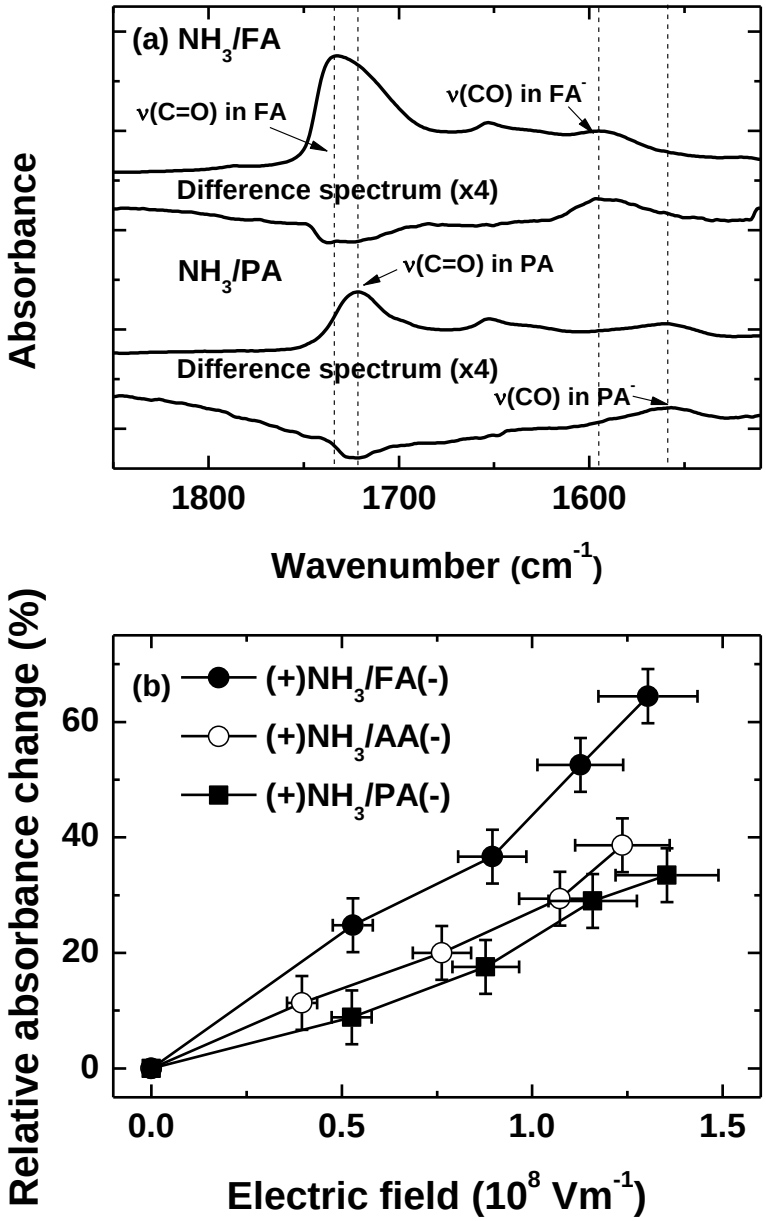


**Figure 4-4.** (a) (Top) RAIR spectrum and field difference spectrum of an $NH_3$(top, 12 ML)/FA(bottom, 19 ML) layered film at F = 1.4 × $10^8$ $Vm^{-1}$. (Bottom) RAIR spectrum and field difference spectrum of an $NH_3$(top, 12

ML)/PA(bottom, 20 ML) layered film at F = 1.4 × $10^8$ $Vm^{-1}$. The difference spectra were magnified by a factor of 4. (b) Relative absorbance changes in the ν(CO) peaks of $FA^-$, $AA^-$, and $PA^-$ as a function of applied field strength. The data for AA is identical to that shown in Figure 4-3(b).

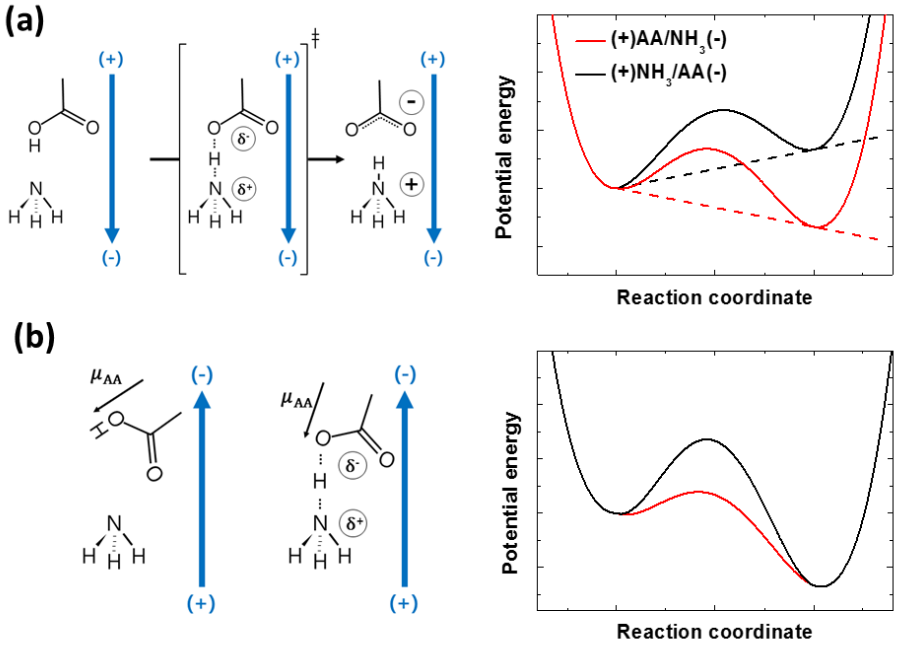


**Figure 4-5.** Illustration of field-induced acid dissociation mechanisms. (a) Electrostatic mechanism. When the OH···N hydrogen bond of the AA-$NH_3$ pair is properly oriented along the field direction, the field facilitates proton transfer from AA to $NH_3$ by electrostatically stabilizing the charged transition state and the product. (b) Reorientation mechanism. The field reorients the AA (or $NH_3$) molecule to provide the AA-$NH_3$ pair with a favorable geometry for spontaneous proton transfer. Note that the field direction is opposite to that of proton transfer via the electrostatic mechanism. The dipole moment of AA is indicated by $\mu_{AA}$.

# Supporting Information

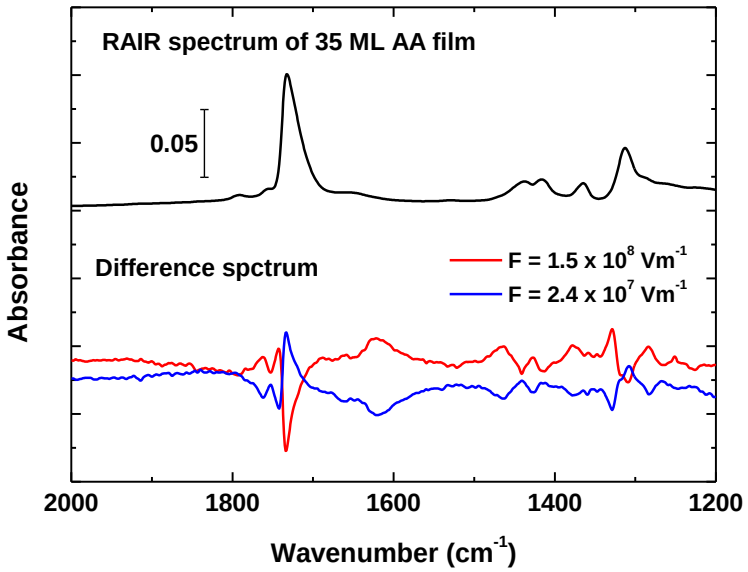


**Figure 4-S1.** (Top) RAIR spectrum of a sandwiched 35 ML AA film. $D_2O$ (40 ML)/AA (35 ML)/$D_2O$ (40 ML)/Pt(111) ν(CO) in $AA^-$ is not shown, which indicates that AA molecule did not dissociate at the AA-D2O interface. (Bottom) Field difference spectra.

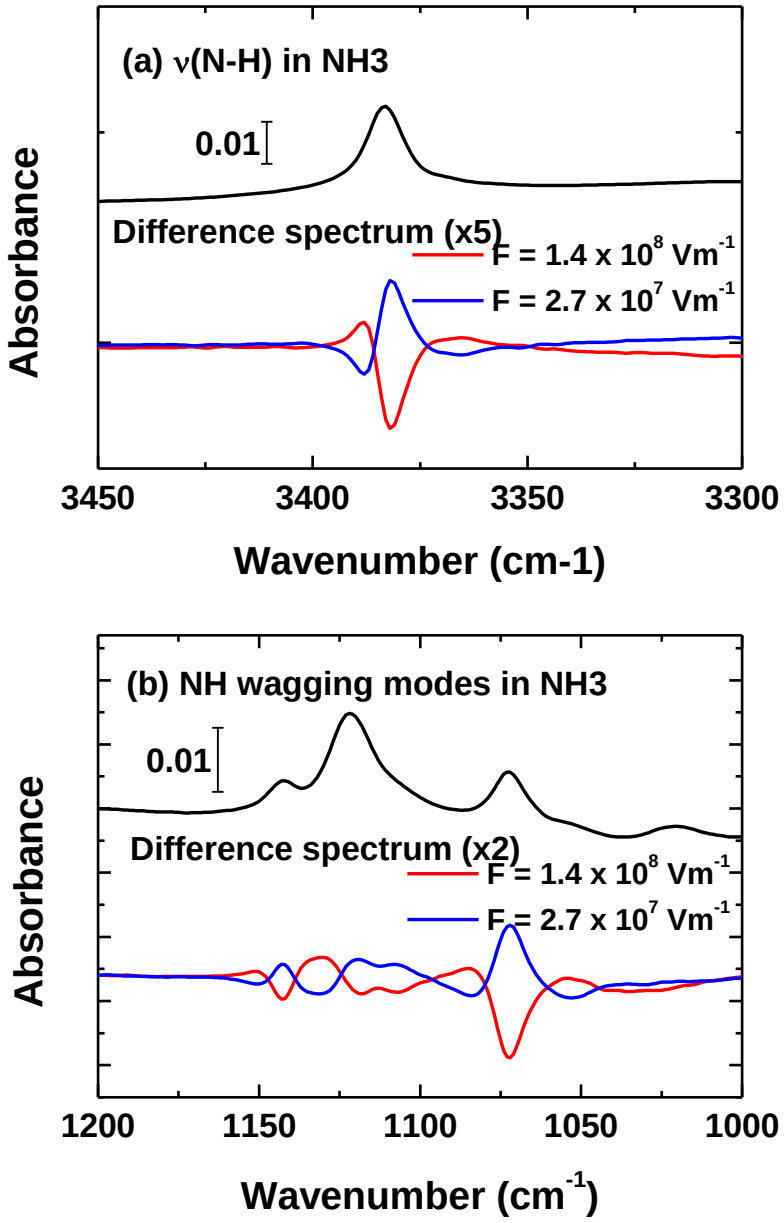


**Figure 4-S2.** RAIR spectrum of an $NH_3$(top, 12 ML)/AA(bottom, 25 ML) layered film. ($D_2O$ (41 ML)/AA (25 ML)/$NH_3$ (12 ML)/$D_2O$ (41ML)/Pt(111)) (a) (Top) RAIR spectrum of the layered film in range of NH Stretching

(Bottom) Field difference spectra. (b) (Top) RAIR spectrum of the layered film in range of NH wagging mode. (Bottom) Field difference spectra.

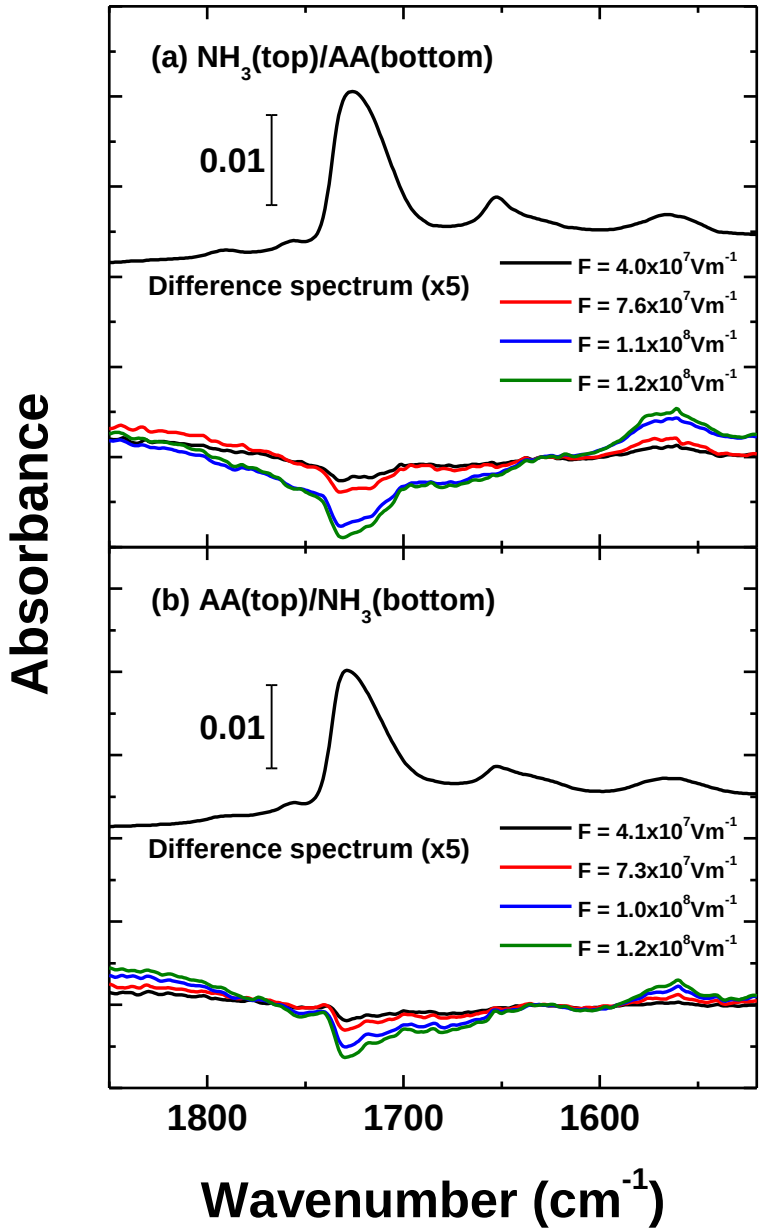


**Figure 4-S3.** (a) (Top) RAIR spectrum of an $NH_3$(top, 12 ML)/AA(bottom, 25 ML) layered film. (Bottom) The field-on minus field-off difference spectra. (b) (Top) RAIR spectrum of an AA(top, 25 ML)/$NH_3$(bottom, 12 ML) layered

film. (Bottom) The field-on minus field-off difference spectra. The difference spectra were magnified by a factor of 5.

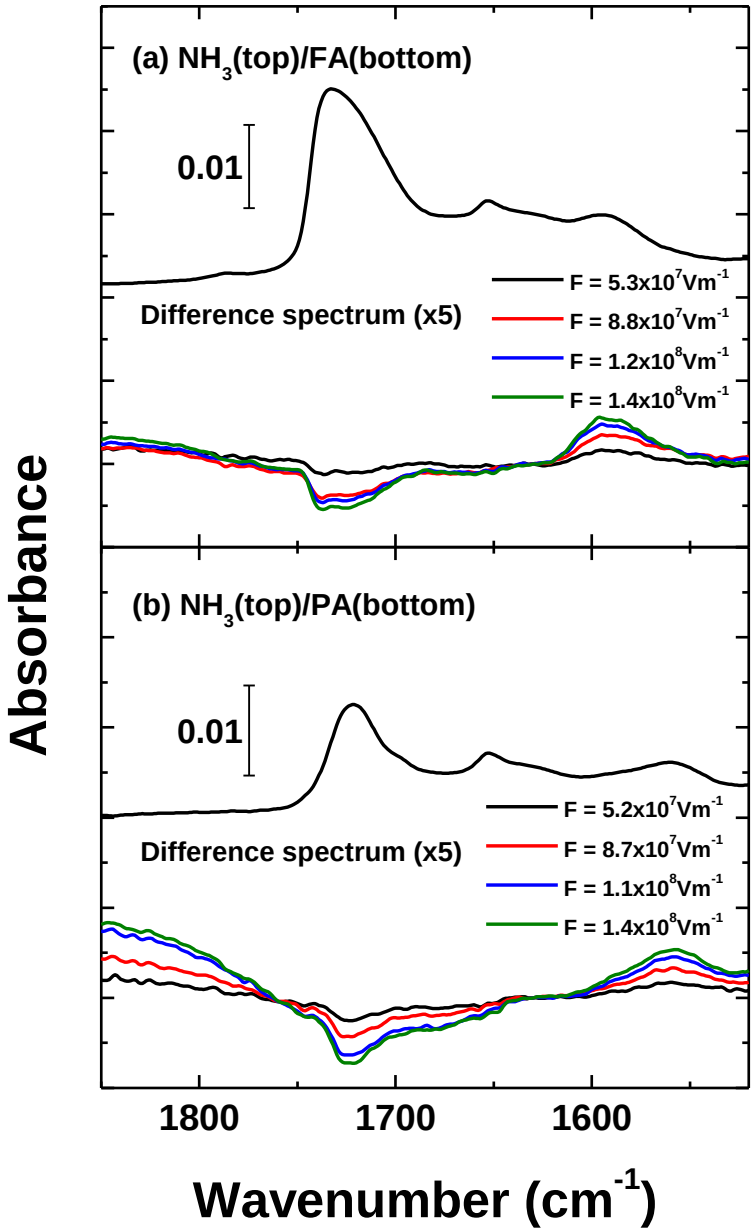


**Figure 4-S4.** (a) (Top) RAIR spectrum of an $NH_3$(top, 12 ML)/FA(bottom, 19 ML) layered film. (Bottom) The field-on minus field-off difference spectra. (b) (Top) RAIR spectrum of an $NH_3$(top, 12 ML)/PA(bottom, 20 ML) layered film.

(Bottom) The field-on minus field-off difference spectra. The difference spectra were magnified by a factor of 5.

# List of Publications

1. Eui-Seong Moon, Youngsoon Kim, Sunghwan Shin and Heon Kang, "Asymmetric Transport Efficiencies of Positive and Negative Ion Defects in Amorphous Ice", *Phys. Rev. Lett.*, 108(22), 226103 (2012)
2. Youngsoon Kim, Eui-seong Moon, Sunghwan Shin, and Heon Kang, "Acidic Water Monolayer on Ruthenium(0001)", *Angew. Chem. Int. Ed.*, 51, 12806 (2012)
3. Sunghwan Shin, Youngsoon Kim, Eui-seong Moon, Du Hyeong Lee, Hani Kang and Heon Kang, "Generation of Strong Electric Fields in an Ice Film Capacitor", *J. Chem. Phys.*, 139, 074201 (2013)
4. Youngsoon Kim, Sunghwan Shin, Eui-Seong Moon and Heon Kang, "Spectroscopic Monitoring of the Acidity of Water Films on Ru(0001): Orientation-Specific Acidity of Adsorbed Water", *Chem. Eur. J.*, 20, 3376 (2014)
5. Sunghwan Shin, Hani Kang, Jun Soo Kim and Heon Kang, "Phase Transitions of Amorphous Solid Acetone in Confined Geometry Investigated by Reflection Absorption Infrared Spectroscopy", *J. Phys. Chem. B*, 118(47), 13349 (2014)
6. Youngsoon Kim, Sunghwan Shin, and Heon Kang, "Zundel-like and Eigen-like Hydrated Protons on a Platinum Surface", *Angew. Chem. Int. Ed.*, 54(26), 7626 (2015)
7. Sunghwan Shin, Youngsoon Kim, Hani Kang, and Heon Kang, "Effect of Electric Field on Condensed-Phase Molecular Systems. I. Dipolar Polarization of Amorphous Solid Acetone", *J. Phys. Chem. C*, 119(27), 15588 (2015)
8. Sunghwan Shin, Hani Kang, Daeheum Cho, Jin Yong Lee and Heon

Kang, “Effect of Electric Field on Condensed-Phase Molecular Systems. II. Stark Effect on the Hydroxyl Stretch Vibration of Ice”, *J. Phys. Chem. C*, 119(27), 15596 (2015)

9. Hani Kang, Sunghwan Shin, Youngwook Park, and Heon Kang, “Effect of Electric Field on Condensed-Phase Molecular Systems. III. The Origin of the Field-Induced Change in the Vibrational Frequency of Adsorbed CO on Pt(111)”, *J. Phys. Chem. C*, 120(27), 17579 (2016)
10. Sunghwan Shin, Youngwook Park, Youngsoon Kim, and Heon Kang, “Dissociation of Trifluoroacetic Acid in Amorphous Solid Water: Charge-Delocalized Hydroniums and Zundel Continuum Absorption”, *J. Phys. Chem. C*, 121(23), 12842 (2017)
11. Sunghwan Shin, Youngwook Park, Youngsoon Kim, and Heon Kang, “Electric Field Effect on Condensed-Phase Molecular Systems. IV. Conformational Change of 1, 2-Dichloroethane” (in preparation)
12. Sunghwan Shin and Heon Kang, “Field -Induced Acid Dissociation at the Acid-Base Interface” (in preparation)

# 요약(국문초록)

본 학위 논문은, 응집계 분자 환경에서 전기장의 효과에 관한 연구 결과를 다루었다. 많은 연구자들이 전기장에 의한 자연현상을 다양한 방식으로 연구해오고 있느나, 제한된 실험법들이 전기장의 세기를 제어하고 측정 할 수 있는 조건을 제공하고 있다. 본 실험실에서는 강한 전기장을 얼음 박막에 걸 수 있는 '얼음 박막 축전법'을 계발하였고, 이를 이용해서 응집계 분자 환경에서 전기장의 효과를 연구하였다.

1 장에서는 현재 전기장 효과를 연구하는데 사용되고 있는 다양한 실험법에 관하여 기술 하였다. 이를 바탕으로 '얼음 박막 축전법'이 기존에 실험법에 비해 가지는 장점을 기술 하였다.

2 장에서는 본 논문에서 사용된 여러 실험 방법에 대하여 기술하였다. '얼음 박막 축전법'의 자세한 실험 방법과 관련 이론에 대해 정리하였고, 분자의 물리적 화학적 변화를 관찰하는데 사용된 반사-흡광 적외선 분광법에 대한 이론을 기술 하였다.

3 장에서는 1,2-디클로로에탄 분자가 전기장에 의해 구조가 변화되는 것을 보이고, 그 변화 정도를 전기장 세기에 따라 정량화하였다. 반사-흡광 적외선 분광법을 이용해서 1,2-디클로로에탄 분자의 고우시/트랜스 변환 및 고우시 1,2-디클로로에탄 분자의 회전 변화를 측정하였다. 트랜스 1,2-디클로로에탄 분자는 전기장에 의해 극성을 가지는 고우시 1,2-디클로로에탄 분자 형태로 변화되었고, 이 변화는 고우시 분자의 이중극자의 전기장 방향으로 정렬을 동반하였다. 이러한 분자의 변화는

50 – 90 K 범위의 온도에서 관찰 되었지만, 8 K에서는 관찰되지 않았다. 이는 정전기적 에너지와 열 에너지가 협력적으로 분자의 형태변화를 야기하는데 관여하는 것을 의미한다.

4 장에서는 아세트산이 전기장에 의해서 분해되는 과정을 '얼음 박막 축전법'을 이용해서 연구한 내용을 기술 하였다. 아세트산의 분해과정은 적외선 분광법을 이용해서 관찰하였고, 이를 통해 밝혀낸 전기장에 의한 산 분해 반응의 메커니즘을 기술 하였다. 아세트산 분자는 산-염기 분자 계면에서 전기장에 의해 아세테이트 이온으로 분해되었다. 전기장에 의해 산 분자가 분해되는 양은 전기장에 방향에 따라 차이를 보였고, 이러한 방향성으로부터 전기장의 의한 산분해 반응이 반응분자의 전기장에 의한 회전에 의해서 촉진됨을 밝혀냈다. 산 분자 크기에 따른 효과를 포름산과 프로피온 산을 이용해서 연구하였고, 산 분자의 크기가 작을수록 전기장에 의한 분해 반응이 잘 일어남을 보였다. 이는 전기장에 의한 산 분해 반응이 분자의 회전에 의해서 일어남을 보여준다.

주요어 : 전기장, 얼음 박막 축전법, 표면 축전, 분자 구조 변화, 산-염기 화학, 분자회전, 반사-흡광 적외선 분광법.

학 번 : 2011-23226